Unveiling the Crucial Role of Pro-inflammatory Macrophages in the Immune Network Imbalance of the maternal-fetal interface with Preeclampsia

Haiyi Fei[#1,2,3], Xiaowen Lu [#1,2,3], Zhan Shi[#1,2,3], Xiu Liu[1,2,3], Cuiyu Yang[1,2,3], Xiaohong Zhu[4], Yuhan Lin[1,2,3], Ziqun Jiang[1,2,3], Jianmin Wang[1,2,3], Dong Huang[1,2,3], Liu Liu[1,2,3], Songying Zhang*[1,2,3] , Lingling Jiang*[1,2,3]

[1]Assisted Reproduction Unit, Department of Obstetrics and Gynecology, Sir Run Run Shaw Hospital, School of Medicine, Zhejiang University, Hangzhou, 310016, China.

[2]Zhejiang Provincial Clinical Research Center for Reproductive Health and Disease, Hangzhou, 310016, China.

[3]Zhejiang Key Laboratory of Precise Protection and Promotion of Fertility, Hangzhou, 310016, China.

[4]Department of Obstetrics and Gynecology, Zhejiang Xiaoshan Hospital, 310016, Hangzhou, China

***Co-corresponding authors**

Lingling Jiang
Assisted Reproduction Unit, Department of Obstetrics and Gynecology,
Sir Run Run Shaw Hospital, Zhejiang University School of Medicine,
310000, Hangzhou, China
E-mail: linglingjiang@zju.edu.cn

Songying Zhang
Assisted Reproduction Unit, Department of Obstetrics and Gynecology,
Sir Run Run Shaw Hospital, Zhejiang University School of Medicine,
310000, Hangzhou, China
E-mail: zhangsongying@zju.edu.cn

Abstract

Preeclampsia (PE), a major cause of maternal and perinatal mortality with highly heterogeneous causes and symptoms, is usually complicated by gestational diabetes mellitus (GDM). However, a comprehensive understanding of the immune microenvironment in the placenta of PE and the differences between PE and GDM is still lacking. In this study, Cytometry by time of flight (CyTOF) indicated that the frequencies of memory-like Th17 cells ($CD45RA^{-}CCR7^{+}IL\text{-}17A^{+}CD4^{+}$), memory-like $CD8^{+}$ T cells ($CD45RA^{-}CCR7^{+}CD38^{+}pAKT^{mid}CD127^{low}CD8^{+}$) and pro-inflam Macs ($CD206^{-}CD163^{-}CD38^{mid}CD107a^{low}CD86^{mid}HLA\text{-}DR^{mid}CD14^{+}$) were increased, while the frequencies of $CD69^{hi}Helios^{mid}CD127^{mid}$ γδT cells, anti-inflam Macs ($CD206^{+}CD163^{-}CD86^{mid}CD33^{+}HLA\text{-}DR^{+}CD14^{+}$) and granulocyte myeloid-derived suppressor

cells (gMDSCs, $CD11b^{+}CD15^{hi}HLA\text{-}DR^{low}$) were decreased in the placenta of PE compared with that of NP, but not in that of GDM or GDM&PE. The pro-inflam Macs were positively correlated with memory-like Th17 cells and memory-like $CD8^{+}$ T cells but negatively correlated with gMDSCs. Single-cell RNA sequencing revealed that transferring the $F4/80^{+}CD206^{-}$ pro-inflam Macs with a $Folr2^{+}Ccl7^{+}Ccl8^{+}C1qa^{+}C1qb^{+}C1qc^{+}$ phenotype from the uterus of PE mice to normal pregnant mice induced the production of memory-like $IL\text{-}17a^{+}Rora^{+}Il1r1^{+}TNF^{+}Cxcr6^{+}S100a4^{+}CD44^{+}$ Th17 cells via IGF1-IGF1R, which contributed to the development and recurrence of PE. Pro-inflam Macs also induced the production of memory-like $CD8^{+}$ T cells but inhibited the production of $Ly6g^{+}S100a8^{+}S100a9^{+}Retnlg^{+}Wfdc21^{+}$ gMDSCs at the maternal-fetal interface, leading to PE-like symptoms in mice. In conclusion, this study revealed the PE-specific immune cell network, which was regulated by pro-inflam Macs, providing new ideas about the pathogenesis of PE.

Introduction

In recent years, low fertility is a global problem (Agbaglo et al., 2022), exacerbated by pregnancy complications. Preeclampsia (PE) is a progressive systemic disease during pregnancy, with pregnancy-induced hypertension, proteinuria, and liver and kidney injury as the main diagnostic indicators (Chappell et al., 2021). With a global prevalence of 7–10%, PE is a major cause of maternal and perinatal mortality and morbidity, especially in low-income and middle-income countries. The only specific treatment is delivery (Chappell et al., 2021). However, due to the variety of symptoms and the heterogeneity of the disease, the pathogenesis of PE is still unclear (Burton et al., 2019; Grotegut, 2016).

PE is often complicated by gestational diabetes mellitus (GDM), which is characterized by insulin resistance and associated with aberrant maternal immune cell adaption (Corrêa-Silva et al., 2018; McElwain et al., 2021; McIntyre et al., 2019). Studies have shown that GDM is an independent risk factor for preeclampsia (Nerenberg et al., 2013; Ostlund et al., 2004; Schneider et al., 2012). However, whether a different pathogenesis underlies between PE and GDM is still unclear.

The fetus is equivalent to a semi-homogenous graft for the mother. Therefore, maternal-fetal immune tolerance plays an important role in the maintenance of pregnancy. Currently, the pivotal mechanism underpinning the pathogenesis of preeclampsia is widely acknowledged to involve an increased frequency of pro-inflammatory M1-like maternal macrophages (Faas et al., 2014; Yao et al., 2019), along with an elevation in granulocytes that capable of superoxide generation (Lampé et al., 2011; D. Liu et al., 2021), $CD56^{+}$ $CD94^{+}$ natural killer (NK) cells (Bachmayer et al., 2006; Travis et al., 2020), $CD19^{+}CD5^{+}$ B1 lymphocytes (Jensen et al., 2012; LaMarca et al., 2011; Zhong et al., 2007), and activated γδ T cells (Chatterjee et al., 2017). Conversely, this pathological process is accompanied by a notable decrease in the frequency of anti-inflammatory M2-like macrophages (Faas et al., 2014; Yao et al., 2019) and $NKp46^{+}$ NK cells (Fukui et al., 2011). Adaptive immune response is also critical for the pathogenesis of PE (Deer et al., 2023). In PE, $CD4^{+}$ T cells prefer to differentiate into pro-inflammatory Th1 and Th17 (Eghbal-Fard et al., 2019; Fu et al., 2014; Lang et al., 2021; Lu et al., 2020; Saito et al. 2007) instead of non-inflammatory Th2 and Treg

(Care et al., 2018; Cornelius et al., 2015a; Saito et al., 2007; Santner-Nanan et al., 2009; Sasaki et al., 2007).

Moreover, PE can be subdivided into early- and late-onset PE diagnosed before 34 weeks or from 34 weeks of gestation, respectively. Research has revealed that among the myriad of cellular alterations in PE, pro-inflammatory M1-like macrophages and intrauterine B1 cells display an augmented presence at the maternal-fetal interface of both early-onset and late-onset PE patients. Decidual natural killer (dNK) cells and neutrophils emerge as paramount contributors, playing a more crucial role in the pathogenesis of early-onset PE (Aneman I et al., 2020). However, a comprehensive and in-depth understanding of the maternal-fetal interface of PE is still lacking.

The immune cells crosstalk with each other at the maternal-fetal interface elaborately. For example, the interaction between B2 cells and Th cells depends on CD40 and its ligand CD40L, which helps B2 cells provide AT1-AAs and differentiate into memory B cells in reducing uterine perfusion pressure (RUPP) rats (Cornelius et al., 2015b). The cytokines derived from NK cells can promote the differentiation of Th17 to co-work in recurrent miscarriage (Fu et al., 2013). The intricate interplay and precise coordination between immune cells are pivotal in maintaining pregnancy. Nevertheless, the regulation of the immune network at the maternal-fetal interface of PE patients still needs to be further studied.

In this study, we combined cytometry by time of flight (CyTOF), single-cell RNA sequencing (scRNA-seq), and rodent experiment to identify the overall immune cell composition and their interactions at the maternal-fetal interface in PE, GDM, and GDM complicated with PE (GDM&PE). This study revealed the PE-specific immune cell network, which was regulated by pro-inflammatory macrophages, providing new ideas about the pathogenesis of PE.

Results

Overall immune cell profile in the placenta of PE, GDM, and GDM&PE

To fully characterize the immune microenvironment at the maternal-fetal interface of PE, we collected full-term placentas of PE and normal pregnancy (NP), and did a CyTOF test (**Table 1**), which panel was shown in **Table 2**. Since PE is usually complicated by GDM, the subjects of GDM and GDM complicated with PE (GDM&PE) were also included. The experimental workflow for CyTOF is shown in the schematic diagram (**Figure 1A**). We found that in addition to the well-known macrophages and T cells, there are also γδ T cells, B cells, NK cells, granulocytes, dendritic cells (DCs), and myeloid-derived suppressor cells (MDSCs). An overall distribution of $CD45^+$ cell subsets in placentas was shown in the t-SNE maps (**Figure 1B**). There were no significant differences in the proportion of these large subpopulations comparing the PE, GDM, GDM&PE group to the NP group (**Figure 1C**). To identify the ten cell subpopulations, CD4, CD8, and γδTCR were used as markers to distinguish $CD4^+$ T cells, $CD8^+$ T cells, and γδ T cells. CD11b is a marker that distinguishes myeloid cells, including macrophages and granulocytes (**Figure 1D**). The ten cell subsets were further annotated by 41 markers in the heatmap (**Figure 1E, Table 3**).

Specific altered T cell profile in the placenta of PE

To gain a comprehensive understanding of the distribution patterns within each cellular

subset, we conducted separate clustering analyses for $CD4^+$T, $CD8^+$T, and γδT cells, respectively. We first analyzed 15 clusters of $CD4^+$ T cells from the placentas of NP, PE, GDM, and GDM&PE (**Figure 2A**). $CD4^+$ T cell clusters were defined by canonical marker set signatures (**Figure 2-figure supplement 1A**). The frequencies of memory-like $CD45RA^-CCR7^{mid}CD28^+CD127^+CD4^+$ T cells (cluster 8) were significantly increased in individuals with PE compared with NP controls. At the same time, there was no significance in the GDM and GDM&PE groups compared with the NP group (**Figure 2B, Table 4**). We analyzed the expression of common intracellular molecules in $CD4^+$ memory-like T cells by sorting $CD45RO^+CCR7^+CD4^+$ T cells from placental samples by flow cytometry. Higher levels of IL-17A and lower levels of Foxp3 were found in memory-like $CD45RO^+CCR7^+CD4^+$ T cells in the placentas of individuals with PE (**Figure 2C**). Consistent with the results of CyTOF, higher fluorescence intensity of $CD45RO^+CD4^+$ T cells was found in the placentas of individuals with PE than that of NP, and this cell population was mainly located in the placental sinusoids (**Figure 2D**), suggesting that these T cells should be recently recruited. Moreover, lower expression of immune checkpoint molecules including T-cell immunoglobulin mucin-3 (Tim-3) and programmed cell death 1 (PD-1) was found in $CD45RA^-CCR7^+CD4^+$ memory T cells in the PE group, suggesting that these cells have a lower immunosuppressive capacity (Chen et al., 2022; Fanelli et al., 2021; Rasmussen et al., 2022; Wang et al., 2016), there was no significant difference in the GDM or GDM&PE groups comparing with the NP group (**Figure 2E**). Then, 18 clusters of $CD8^+$ T cells were analyzed (**Figure 2F**). $CD8^+$ T cell clusters annotation was based on the expression of canonical marker signatures (**Figure 2-figure supplement 1B**). $CD45RA^-CCR7^+CD38^+pAKT^{mid}CD127^{low}$ (cluster 2) memory-like $CD8^+$ T cells were significantly increased in the PE group (**Figure 2G, Table 4**). Cluster 2 of the PE group expressed lower levels of PD-1 and TIGIT, suggesting the activation of cytotoxicity of these cells (**Figure 2H**) (Morita et al., 2020). Then, 22 clusters of γδT cells were analyzed and annotated (**Figure 2I, Figure 2-figure supplement 1C**). Cluster 15, with lower expression of Tim3, was significantly decreased in the PE group (**Figure 2J, 2K**). Nevertheless, neither the $CD4^+$ T cells nor the $CD8^+$ T cells exhibited any alteration in the memory-like clusters when comparing the GDM or GDM&PE groups to the NP group.

In conclusion, significant changes in placental T cell profile were found in the placentas of PE but not in those of GDM or GDM&PE, suggesting that abnormal activation of T cells in the placenta is associated with the pathogenesis of PE.

Abnormal polarization of macrophages was correlated with specific immune cell subsets in individuals with PE

Except for T cells, we also analyzed 29 clusters of $CD45^+CD3^-CD11b^+$ cells from placentas of NP, PE, GDM, and GDM&PE, including 9 clusters of macrophages, 11 clusters of granulocytes, and 5 clusters of NK/NK-like cells (**Figure 3A**). The clusters of $CD45^+CD3^-CD11b^+$ cells were defined by canonical marker set signatures (**Figure 3B**). Moreover, significantly decreased frequencies of $CD11b^+CD15^{hi}$HLA-DR^{low} granulocytes (cluster 12), which are identified as granulocyte myeloid-derived suppressor cells (gMDSCs), were found in the PE group (**Figure 3C, Table 4**). In addition, the frequency of anti-inflammatory macrophages (anti-inflam Macs) ($CD206^+CD163^-CD86^{mid}CD33^+$HLA-$DR^+$, cluster 25) was also significantly decreased, whereas the frequency of pro-inflammatory macrophages (pro-inflam Macs) ($CD206^-CD163^-CD38^{mid}CD107a^{low}CD86^{mid}$HLA-$DR^{mid}CD14^+$,

cluster 23) was significantly increased in the PE group (**Figure 3C, Table 4**). However, the frequencies of macrophages and gMDSCs were unchanged significantly in the GDM or GDM&PE groups.

Pearson correlation analysis indicated positive correlations between pro-inflam Macs (cluster 23 in $CD11b^+$ cells) and $CD4^+$ memory-like T cells (cluster 8 of $CD4^+$ T cells), as well as $CD8^+$ memory-like T cells (cluster 2 in $CD8^+$ T cells). $CD206^-$ pro-inflam Macs were negatively correlated with gMDSCs (cluster 12 in $CD11b^+$ cells), but were not statistically significant. Conversely, $CD206^+$ anti-inflam Macs (cluster 25 in $CD11b^+$ cells) were positively correlated with gMDSCs and negatively correlated with $CD8^+$ memory-like T cells (**Figure 3D, 3E**).

These results suggested that abnormally polarized $CD206^-$ pro-inflam Macs are positively correlated with memory-like $CD4^+$ and $CD8^+$ T cells in the placentas of individuals with PE and negatively correlated with gMDSCs.

$F4/80^+CD206^-$ pro-inflam Macs induced immune imbalance at the maternal-fetal interface and PE-like symptoms

Though increased pro-inflam Macs have been reported in the placenta from individuals with PE (Faas et al., 2014), few studies have reported the interaction between macrophages and other immune cells in the placenta. In this study, transcriptome RNA-seq was used to analyze the difference between $CD45^+F4/80^+CD206^-$ pro-inflam Macs and $CD45^+F4/80^+CD206^+$ anti-inflam Mac isolated from the uterus and placentas of mice with reducing uterine perfusion pressure (RUPP) (**Figure 4A**). The diagrammatic representation of the RUPP model is presented in Figure 4-figure supplement 1A. To establish the PE mouse model, we ligated uterine arteries in pregnant mice on day 12.5 of gestation, and mice with sham operation were considered as controls (**Figure 4-figure supplement 1A**). We found that mice of RUPP showed an increased embryo absorption rate, decreased fetal weight, and pup crown-rump length compared with the sham operation group (**Figure 4-figure supplement 1B**). Increased systolic blood pressure (SBP) and urine albumin creatine ratio (UACR) were also observed in mice with RUPP, which indicated a successful PE mice mode was built (**Figure 4-figure supplement 1C**). In addition, the green fluorescent protein (GFP) pregnant mice were used to distinguish between maternal and fetal derived macrophages. The wild-type (WT) female mice were mated with either transgenic male mice, genetically modified to express GFP to generate either GFP-expressing pups (GFP^+pups), or mated with WT male mice for control (**Figure 4-figure supplement 1D**). We found that the majority of macrophages in the uterus and placenta are of maternal origin ($CD11b^+GFP^-$). In contrast, fetal-derived macrophages ($CD11b^+GFP^+$) represent a mere fraction of the total macrophage population (**Figure 4-figure supplement 1E**). In light of these findings, we have incorporated mouse uterine tissues to isolate macrophages for subsequent experiments with enhanced effectiveness.

Significant differences were found between the pro-inflam and anti-inflam macrophages derived from RUPP mouse (**Figure 4B**). There are 2123 genes increased, and 2699 genes decreased significantly in the pro-inflam Macs compared to the anti-inflam Macs (**Figure 4C**). The expression levels of genes associated with inflammatory response (Ccl7, Ccl8, Ccl2, IL6) (He et al., 2019; Wu et al., 2023), complement system activation (C1qa, C1qb) (Chen et al., 2021), and lipid metabolism (Pltp, Apoe) (Desrumaux et al., 2016) were significantly increased in the pro-inflam Macs; whereas the expression levels of genes associated with the regulation

of angiogenesis and vascular endothelial growth factor production (VEGFα, Macro) and tissue development (TGF-β1, Thbs1, Fn1, Slpi) (Jin et al., 2023; Nugteren et al., 2021; Li et al., 2022) were significantly decreased (**Figure 4C, 4D**). Moreover, Gene Set Enrichment Analysis (GSEA) was performed to explore the most significantly enriched functional terms between the two groups of macrophages. We found that NF-κB signaling and interspecies interaction between organisms were enriched in the pro-inflam Macs, while tissue development and epithelial cell morphogenesis were enriched in the anti-inflam Macs (**Figure 4E**).

To further investigate the effect of the pro-inflam Macs in immune imbalance at the maternal-fetal interface, PLX3397, the inhibitor of CSF1R, which is needed for macrophage development, was used to deplete the macrophages of pregnant mice (X. Chen et al., 2023; J. Chen et al., 2022) (**Figure 4-figure supplement 2A**). As expected, an increased embryo resorption rate, decreased fetal top-rump length and fetal weight were found in mice injected with pro-inflam Macs (**Figure 4F**). Increased SBP and UACR were also found in mice injected with pro-inflam Macs (**Figure 4G**). Moreover, it is shown that $CD44^+$ memory-like Th17 cells and memory-like $CD8^+$ T cells increased while $CD11b^+Ly6G^+$ gMDSCs decreased in mice injected pro-inflam Macs compared with mice injected anti-inflam Macs, which validated our findings with CyTOF (**Figure 4H**). Clodronate liposomes were also used to deplete the macrophages of pregnant mice (X. Liu et al., 2022) before pro-inflam Macs or anti-inflam Macs were injected into the mice. The same experimental results were obtained (**Figure 4-figure supplement 2B-2E**). In conclusion, the $F4/80^+CD206^-$ pro-inflam Macs induced immune imbalance at the maternal-fetal interface and PE-like symptoms.

Pro-inflam Macs and anti-inflam Macs subsets are phenotypically heterogeneous

To further explore the role that macrophages play in the immune imbalance at the maternal-fetal interface in PE, scRNA-seq was performed to analyze the $CD45^+$ immune cells in the uterus and placenta from mice that were transferred with pro-inflam Macs or anti-inflam Macs from the uterus and placentas of RUPP mice. An unsupervised cluster detection algorithm (SEURAT) was applied and eight types of immune cells were detected by mostly distinguishable cell type-specific genes, including macrophages, monocytes, granulocytes, T/NK cells, B cells, DC-like cells, mast cells, and basophils (**Figure 5A, 5B**).

Macrophages were further identified into 15 clusters defined by marker set signatures. Single-cell differential expression analysis (SCDE) was performed for each population and characteristic gene expression patterns were detected for cluster 0-cluster 14 to characterize the phenotypes of these subsets in detail ((**Figure 5C**). We found that the frequency of cluster 0 was significantly increased in mice injected with pro-inflam Macs, while the frequency of cluster 1 was significantly decreased (**Figure 5D**). We also found that cluster 0 highly expresses genes associated with fetal and tissue resident (Folr2) (Nalio et al., 2022; Thomas et al., 2021), complement system activation (C1qa, C1qb, C1qc) (Chen et al., 2021), and inflammatory response (Ccl7, Ccl8) (He et al., 2019; Wu et al., 2023); while cluster 1 highly expresses genes associated with tissue repair (Chil3, Slpi, Fn1) (Jin et al., 2023; Nugteren et al., 2021; Li et al., 2022), blood vessel morphogenesis (Thbs1) (Che et al., 2021) and preventing oxidative stress (Gsr, Mgst1) (Coppo et al., 2022) (**Figure 5E**). Changes in gene expression patterns of cluster 0 (pro-inflam Macs) and cluster 1 (anti-inflam Macs) were analyzed in mice injected the pro-inflam Macs or anti-inflam Macs. We found that enriched GO terms in cluster 0 and cluster1 including ‘antigen processing and presentation of

exogenous antigen' and 'inflammatory response' in the pro-inflam Macs group (**Figure 5F**), in which high expression of genes such as CCL5, CCL8, CALR, IRF7, IL10, IFI44, IFI30, OAS3, etc. could be observed (**Figure 5G**). The control group showed elevated expression of MMP14, Chil3, EGR1, ATF3 and VASP (**Figure 5G**); and these genes were enriched in 'vascular endothelial growth factor production' and 'tissue development' (**Figure 5F**). These results were consistent with the transcriptome RNA sequencing results of macrophages.

These data suggested that the $CD45^{+}F4/80^{+}CD206^{-}$ pro-inflam Macs with a $Folr2^{+}Ccl7^{+}Ccl8^{+}C1qa^{+}C1qb^{+}C1qc^{+}$ phenotype play an important role in the development of PE.

Pro-inflam Macs induced the memory-like Th17 cells, which was associated with the development and recurrence of PE

We also analyzed the scRNA-seq data of uterine T/NK cells from mice that were injected with or without pro-inflam Macs. T/NK cells were further identified into 12 clusters defined by marker set signatures (**Figure 6A,6B**). We found that the frequency of cluster 0 was increased in mice injected with pro-inflam Macs, while the frequency of cluster 1 and cluster 2 were significantly decreased (**Figure 6A**). In addition to genes associated with Th17 cells (IL-17a, IL17f, Rora, Il1r1, TNF) (Wu et al., 2019; Leite et al., 2023), cluster 0 also exhibits high expression of genes associated with memory phenotype (Cxcr6, S100a4, CD44) (Schroeder et al., 2023; Bieberich et al., 2021), suggesting that cluster 0 was the memory-like Th17 cells (**Figure 6C**). Cluster 1 exhibited high expression of genes associated with immunoregulation (Lef1, Tcf7, Ccr7) (Qiu et al., 2022; Sekine et al., 2020); Cluster 2 exhibited high expression of genes associated with immunomodulation (Gata3, GITR, CD28), suggesting that cluster 1 and 2 were T cells with immunomodulation function (Esensten et al., 2016; Pai et al., 2023) (**Figure 6C)**. Changes in gene expression patterns of cluster 0 (memory-like Th17 cells) were analyzed in the pro-inflam Macs group and control group. We found that in the pro-inflam Macs group, enriched GO terms including 'positive regulation of response to external stimulus' and 'tumor necrosis factor production' (**Figure 6D**), in which highly express genes such as TNFSF11, TNF, IL27RA, IGF1R, CD226, LAMP1 (**Figure 6E**). The control group showed elevated expression of ASS1, EIF5, S100A9, CTLA4, S100A8 and CXCR4 (**Figure 6E**); these genes were enriched in GO terms including 'regulation of programmed cell death' and 'cellular biosynthetic process' (**Figure 6D**). In summary, the pro-inflam Macs induced memory-like Th17 cells, which were characterized by $IL\text{-}17a^{+}IL17f^{+}Rora^{+}Il1r1^{+}TNF^{+}Cxcr6^{+}S100a4^{+}CD44^{+}$.

To confirm the importance of memory-like $CD4^{+}$ T cells in the pathogenesis of PE, the $CD4^{+}CD44^{+}$ T cells in the uterus and placentas from RUPP or NP mice were sorted and intravenously injected into normal pregnant mice on day12.5 of gestation (**Figure 6F**). The $CD4^{+}CD44^{+}$ T cells derived from RUPP mouse were characterized by an increased frequency of Th17 cells and a reduced frequency of Tregs (**Figure 6F**). Increased embryo absorption rate, decreased fetal weight and pup crown-rump length were found in mice injected with PE mouse-derived $CD4^{+}CD44^{+}$ T cells (**Figure 6G**). The PE-like symptoms, including increased SBP and UACR, were also observed in those mice (**Figure 6H**).

It has been reported that sustained expansion of immunosuppressive memory Tregs during prior pregnancy is beneficial for maintaining a second pregnancy (Rowe et al., 2012). To verify whether memory-like Th17 cells promote the recurrence of PE, we established a second pregnant mouse model with a history of PE or NP in the first pregnancy. An increased embryo

resorption rate, decreased crown-rump length, and fetal weight were found in mice with a history of PE pregnancy compared with those with a history of NP pregnancy (**Figure 6-figure supplement 1A**). Moreover, mice with a history of PE in the first pregnancy showed increased SBP and UACR during the second pregnancy (**Figure 6-figure supplement 1B**). Consistently, higher levels of IL-17A were also found in memory-like $CD4^+$ T cells in mice with a history of PE in the first pregnancy (**Figure 6-figure supplement 1C**). Therefore, pro-inflam Macs induced the IL-$17a^+$IL$17f^+$$Rora^+$$Il1r1^+$$TNF^+$$Cxcr6^+$$S100a4^+$$CD44^+$ memory-like Th17 cells, which was associated with the development and recurrence of PE.

Pro-inflam Macs lead to a reduced proportion of gDMSCs

The uterine granulocytes from mice that were transferred with pro-inflam Macs from PE mice were further analyzed using scRNA-seq. Granulocytes were identified into 12 clusters defined by marker set signatures (**Figure 6-figure supplement 2A, 2B**). We found that cluster 0-cluster 3 were different between the two groups: the frequency of cluster 0 and cluster 2 were increased in mice injected with pro-inflam Macs, while the frequency of cluster 1 and cluster 3 were decreased (**Figure 6-figure supplement 2A**)). Cluster 0 had the signature of a mature granulocyte (FOS, FOSB) (Montaldo et al., 2022), and also highly expressed IL-1R2 and CSF3R; Cluster 1 highly expressed genes associated with immunoregulation genes (Hmox1, CCL4, CCL3, Lcn2) (Wenzel et al., 2022; Montaldo et al., 2022); Cluster 2 highly expressed pro-inflammatory genes (IFITM1, IL1B, Ptgs2, Cxcl3) (Ulff-Møller et al., 2018; Drummond al., 2022); while cluster 3 highly expressed gMDSCs associated genes (Ly6g, S100a8, Retnlg, Wfdc21) (von Wulffen et al., 2023; Kao al., 2023) (**Figure 6-figure supplement 2C**). Our animal experiments above (Figure 4) have identified a reduced proportion of $CD11b^+$$Ly6G^+$ gMDSCs in the mice injected with pro-inflam Macs. Changes in gene expression patterns of cluster 3 (gMDSCs) were analyzed in the pro-inflam Macs group and the control group. Enriched GO terms including 'tumor necrosis factor production' and 'leukocyte mediated immunity' were found in the pro-inflam Macs group (**Figure 6-figure supplement 2D**), which highly express the genes such as IRF7, EGR1, C1QA, C1QB, CCL2, CSF3R, TNFRSF1B (**Figure 6-figure supplement 2E**). The control group showed elevated expression of CCL4, CXCL10, CD177, MMP8, S100A13, LCN2 and SPP1 (**Figure 6-figure supplement 2E**); these genes were enriched in 'granulocyte migration' and 'localization' (**Figure 6-figure supplement 2D**). Except for gMDSCs, we also revealed a pronounced increase in the proportion of $CD15^+$$CD66b^+$ neutrophils among PE patients, implying the importance of neutrophils in the development of PE (Akkari L et al., 2024) (**Figure 6-figure supplement 2F**).

In conclusion, from the rodent experiments and the data of scRNA-seq, we demonstrated that pro-inflam Macs suppressed the production of $Ly6g^+$$S100a8^+$$Retnlg^+$$Wfdc21^+$ gMDSCs.

Pro-inflam Macs induced the production of memory-like Th17 cells via IGF1-IGF1R

Our results above showed that pro-inflam Macs induced memory-like Th17 cells in PE, however, the underlying molecular mechanisms were still unknown. CellPhoneDB analysis indicated that increased communication counts and signaling pathways numbers between macrophages and T/NK cells were observed in mice injected with pro-inflam Macs (**Figure 7—figure supplement 1A, 1B**). Then we identified the interacting ligand-receptor pairs between different types of immune cells and macrophages. Insulin-like growth factor 1 (IGF1) -IGF1 receptor (IGF1R) ligand-receptor pair was significantly enhanced between

macrophages and T/NK cells in mice injected with pro-inflam Macs (**Figure 7A**). IGF1 has significant effects on immune function maintenance, and signaling through IGF1R could cause increased aerobic glycolysis, favoring Th17 cell differentiation over that of Treg cells (Bekkering et al., 2018; DiToro et al., 2020). For further demonstration, we analyzed the frequencies of $IGF1^+CD14^+$ cells and $IGF1R^+CD4^+$ cells in placentas of individuals with PE and NP and found both of these two cells were significantly increased in the PE group (**Figure 7B**).

Trophoblast-derived extracellular vesicles from the placenta of PE (PE-EVs), which carry the fetal antigen, could induce M1-like macrophage (pro-inflammatory Macs) polarization to participate in the development of PE according to our previous study (X. Liu et al., 2022). To confirm whether pro-inflammatory Macs induced the production of memory-like Th17 cells via IGF1-IGF1R, macrophages from human peripheral blood, after incubating with PBS, trophoblast-derived extracellular vesicles from NP (NP-EVs) or PE-EVs in vitro, were co-cultured with $CD4^+$ naïve T cells (**Figure 7C**). The frequencies of memory-like $CD45RO^+$ $CCR7^+$ IL-$17A^+$ $CD4^+$ cells significantly increased in the PE-EVs-induced macrophages group rather than in the NP-EVs-induced macrophages group. However, the frequencies of memory-like Th17 cells significantly decreased after $CD4^+$ naïve T cells were treated with the IGF1R inhibitor BMS-754807 (**Figure 7D**).

To investigate the role of IGF1-IGF1R in the development of PE in vivo, $CD45^+CD4^+$ T cells from NP mice were isolated and treated with BMS-754807 or PBS, then injected into NP mice at day 11.5 of gestation (**Figure 7E**). Lipopolysaccharide (LPS)-induced PE mice model was constructed by intraperitoneal injection of LPS on day12.5 and day15.5 of gestation (Han et al., 2021), and an anti-CD4 antibody was used to deplete the $CD4^+$ T cells in pregnant mice. The mice injected with $CD4^+$ T cells treated by BMS-754807 presented decreased embryo resorption rate and increased pup crown-rump length and fetal weight (**Figure 7F**), decreased SBP and UACR (**Figure 7G**), and decreased frequency of memory-like Th17 cells at the maternal-fetal interface (**Figure 7H**). These data suggested that pro-inflam Macs could induce the production of memory-like Th17 via the IGF1-IGF1R, leading to the development of PE.

Discussion

Preeclampsia, a progressive systemic disease during pregnancy, is closely related to the alterations in the immune environment at the maternal-fetal interface. In this study, the overall immune cell profiles in the placenta of individuals with NP, PE, GDM and GDM&PE were detected by CyTOF and a PE-specific change in immune microenvironment of maternal-fetal interface was described for the first time. Further, we provided a novel insight that pro-inflam Macs induced memory-like Th17 cells, memory-like $CD8^+$ T cells, and suppressed the production of gMDSCs in mice maternal-fetal interface by scRNA-seq. In addition, we first validated that IGF1-IGF1R was involved in producing memory-like Th17 cells induced by pro-inflam Macs in vitro and in vivo, thus leading to the development of PE.

Various studies represented the effect of a single subset of immune cells in the pathogenesis of PE or GDM (Bachmayer et al., 2006; Care et al., 2018; Cornelius et al., 2015a; Eghbal-Fard et al., 2019; Faas et al., 2014; Fu et al., 2014; Fukui et al., 2011; Lampé et al., 2015; Lampé et al., 2011; Lang et al., 2021; D. Liu et al., 2021; Lu et al., 2020; Santner-Nanan et al., 2009; Sasaki et al., 2007; Travis et al., 2020; Yao et al., 2019). Miller et al. provided an overall analysis of immune cells in the human placental villi in the presence and absence of spontaneous labor at term by scRNA-seq (Miller et al., 2022). Fangyuan Luo et al. unveiled the

intricate interplay existing between SPP1^{+}M1 cells and the IGFBP1^{+}SPP1^{+} extracellular villous trophoblast in the context of PE by using sc-RNA seq (Luo F et al., 2023). Li Y et al. highlighted a key role of a distinct perivascular inflammatory CD11c^{high} decidual macrophages subpopulation in the pathogenesis of preeclampsia through sc-RNA sequencing (Li Y et al., 2024). However, The immune cells crosstalk with each other at the maternal-fetal interface elaborately. A comprehensive and in-depth understanding of the immune microenvironment at the maternal-fetal interface of PE is still lacking. Here, we used CyTOF and scRNA-seq to comprehensively analyze the immune cell profile and explore the interaction of immune cells in PE. Additionally, most previous studies have reported immune cells from maternal systemic circulation rather than directly from the tissue of maternal-fetal interface (Cornelius et al., 2015b; Deer et al., 2021; Santner-Nanan et al., 2009; Shields et al., 2018; Wallace et al., 2012). In this study, cells were directly isolated from the tissue of maternal-fetal interface, which is considered as a more accurate approach to unveil the real immune environment of the maternal-fetal interface.

Abnormal inflammatory responses were reported to play an important role in the pathogenesis of both PE and GDM (Aneman et al., 2020; Corrêa-Silva et al., 2018; Deer et al., 2023; Jung et al., 2022; McElwain et al., 2021). However, it is unclear how the maternal-fetal interface immune microenvironment differs between the two diseases. We analyzed the overall placental immune cell profile in NP, PE, GDM and GDM&PE by CyTOF and revealed a PE-specific immune cell profile: The frequencies of memory-like Th17 cells (CD45RA^{-}CCR7^{+}IL-17A^{+}CD4^{+}), memory-like CD8^{+} T cells (CD45RA^{-}CCR7^{+}CD38^{+}pAKT^{mid}CD127^{low}CD8^{+}) and pro-inflam Macs (CD206^{-}CD163^{-}CD38^{mid}CD107a^{low}CD86^{mid}HLA-DR^{mid}CD14^{+}) were increased, while the decreased frequencies of CD69^{hi}Helios^{mid}CD127^{mid} γδT cells, anti-inflam Macs (CD206^{+}CD163^{-}CD86^{mid}CD33^{+}HLA-DR^{+}CD14^{+}) and granulocyte myeloid-derived suppressor cells (gMDSCs, CD11b^{+}CD15^{hi}HLA-DR^{low}) were observed in the placenta of PE, but not in that of GDM or GDM&PE compared with that of NP.

PE is often divided into two subtypes based on the time of onset. Late-onset PE, occurring at 34 weeks of gestation or later, accounts for most preeclampsia cases, while early-onset PE, occurring before or at 33 weeks of gestation (Lisonkova and Joseph, 2013). However, our previous study observed no significant difference in the M1/M2 macrophage polarization in placentas with early-onset or late-onset PE (X. Liu et al., 2022). Therefore, our research was conducted regardless of the preeclampsia-onset type to ensure consistency in macrophage polarization of the two subtypes.

There have been studies indicating that pro-inflammatory macrophages, Th17 cells and CD8^{+} T cells play an essential role in PE development (Care et al., 2018; Eghbal-Fard et al., 2019; Lager et al., 2020; Yao et al., 2019). Macrophages was indicated with a pro-inflammatory phenotype in the placenta with PE (Faas et al., 2014; Yao et al., 2019). Care et al. reported that placental Tregs helped suppress inflammation at the maternal-fetal interface (Care et al., 2018). Similarly, Lu et al. found an abnormal increase of IL-17A in the placenta in the development of PE (Lu et al., 2020). Meanwhile, the abnormal infiltration of CD8^{+} T cells in the placenta may contribute to PE (Lager et al., 2020). Consistent with the previous findings, we found that memory-like CD4^{+} and memory-like CD8^{+} T cells significantly increased in the PE group and that IL-17A was significantly higher expressed in CD4^{+}

memory-like T cells from the PE group, which is vital in vascular inflammation, leading to the development of PE (Amador et al., 2014; Madhur et al., 2021). Though memory T cells play a key role in fetal-maternal tolerance in normal pregnancy (Kieffer et al., 2019), few studies have reported the characteristics of memory-like T cells in the development of PE.

We constructed an adoptive transferred mouse model. The injection of $CD4^+$ T cells from RUPP mouse, characterized by an increased frequency of Th17 cells and a reduced frequency of Tregs, induced PE-like symptoms in pregnant mice. Tregs which are well known to undergird maternal tolerance of the fetus, and which are well known to have an overlapping developmental trajectory with $RORgt^+$ Th17 cells (Robertson SA et al., 2019; Sefik E et al.,2015). This study underscores the importance of Th17/Treg cell balance in maintaining pregnancy homeostasis. And it is worth noting that we isolated $CD4^+$ memory-like T cells directly from the maternal-fetal interface, which is different from previous studies that the $CD4^+$ T cells for adoptive transfer were isolated from the spleen and induced in vitro (Cornelius et al., 2015b; Deer et al., 2021; Shields et al., 2018; Wallace et al., 2012). Recurrence is an important concern in individuals with PE (Bernardes et al., 2019). We found that a prior PE pregnancy increased the probability of PE in the next pregnancy in mice, accompanied by an increased frequency of memory-like Th17 cells at the maternal-fetal interface, suggesting that increased memory-like Th17 cells are positively related to the recurrence of PE. However, further studies are needed to confirm the function of the fetal-specific memory Th17 cells in the recurrence of PE.

Activation of $CD8^+$ T cells and Th1 cells can be induced by abnormal polarized macrophages in recurrent miscarriage (Li et al., 2022). The gMDSCs have been reported to have immune suppressive activity and are necessary for maintaining maternal-fetal tolerance (Köstlin-Gille et al., 2019; Zhou et al., 2018). However, the correlation between macrophages and other immune cells in the development of PE remained unclear. We verified that pro-inflam Macs induced memory-like Th17 cells and memory-like $CD8^+$ T cells and inhibited the production of gMDSCs in PE by correlation analysis and adoptive transfer in animal experiments for the first time, indicating that the immune cells orchestrate a network in the maternal-fetal interface elaborately. However, PLX3397, used in this study, emerges as a promising small-molecule compound, endowed with the capability to traverse the placental barrier, thereby potentially influencing the development and function of fetal macrophages. In addition to gMDSCs, we conducted immunofluorescence analysis of placental tissue, specifically targeting $CD66b^{high}$ neutrophils. Our findings revealed a pronounced increase in the proportion of neutrophils among PE patients, fostering the hypothesis that IL-17A produced by Th17 cells might orchestrate the migration of neutrophils towards the placental milieu. This migratory response, in turn, could potentially trigger reactive oxygen species (ROS)-mediated immunopathology, which subsequently lead to PE (Akkari L et al., 2024).

The function of IGR1 and IGF1R in PE is controversial. IGF1 plays a significant role in maintaining immune function, and IGF1R facilitates the differentiation of naïve $CD4^+$ T cells into Th17 cells (DiToro et al., 2020). A study showed that IGF-1R was downregulated in the serum of individuals with PE (Liao et al., 2021). Decreased amounts of IGF1R were also found in the placentas of individuals with PE (Robajac et al., 2015). However, another study found no significance in the affinity and the number of IGF-1R between placentas from individuals with PE or not (Díaz et al., 2005). We found that mice exhibiting PE symptoms had significantly

enhanced IGF1-IGF1R interaction between inflammatory macrophages and memory-like Th17 cells by analyzing the data of scRNA-seq. Then, this finding was further confirmed in human placentas from individuals with PE and NP, for the frequencies of $IGF1^+$ $CD14^+$ cells and $IGF1R^+$ $CD4^+$ cells were found to significantly increase in the PE group. In vitro, we found that PE-EVs-treated macrophages secreted more IGF1 than NP-EV-treated macrophages and induced a higher frequency of memory-like Th17 cells. The inhibition of IGF1R on $CD4^+$ naïve T cells resulted in a decreased frequency of memory-like Th17 cells, implying that the IGF1-IGF1R is critical for the production of memory-like Th17 cells induced by inflammatory macrophages. Animal experiments confirmed that IGF1R inhibition on $CD4^+$ T cells at the maternal-fetal interface reduced the frequency of memory-like Th17 cells and relieved PE-like symptoms.

In addition, placentas from different groups for CyTOF analysis and flow cytometry were matched by age, preterm pregnancies, and previous abortion history; however, there are differences in body mass index (BMI), gestational age, term pregnancies, and the number of living children. Obesity can increase inflammatory and oxidative stress markers in the placental environment (Spradley et al., 2015). Also, it has been reported that the placental immune state shifts with gestational age (Lewis et al., 2018). However, as PE is often accompanied by obesity and early termination of pregnancy, it is difficult to exclude these factors in sample collection. Moreover, limited placental samples in the GDM&PE group are the shortage of this study, for it is hard to collect enough clean samples that exclude interference factors because the number of pregnant women exposed to COVID-19 has increased sharply since December 2022 in China.

In summary, this study demonstrated the statistically distinguished placental immune microenvironment in individuals with PE, but not in those with GDM or GDM&PE. More importantly, macrophages orchestrate a network in the maternal-fetal interface elaborately. These findings provide novel insights into PE pathogenesis and a potential immune target for the clinical prevention and treatment of PE.

Materials and Methods

Clinical sample collection

The samples used in this study were collected from Sir Run Run Shaw Hospital between October 2020 and August 2023. Informed consent was obtained from all volunteers, and the Ethics Committee of Sir Run Run Shaw Hospital, Zhejiang University School of Medicine, approved the study. Human placentas were obtained from women with NP, PE, GDM, or GDM&PE who underwent elective cesarean delivery. The diagnostic criteria for PE included new-onset hypertension after 20 weeks of gestation with SBP ≥140 mmHg and/or diastolic blood pressure ≥90 mmHg and proteinuria (≥300 mg) on at least two occasions. A positive glucose tolerance test diagnoses gestational diabetes mellitus. Women with normal blood pressure, full-term pregnancies, and no complications were designated as controls. The detailed clinical characteristics of the pregnant women in this study are presented in Table 5 and Table 6.

Mice

Eight-week-old female C57 mice and ten-week-old male BALB/c mice were purchased

from Hangzhou Ziyuan Laboratory Animal Technology Co., Ltd (Hangzhou, China) and Shanghai Jihui Experimental Animal Breeding Co., Ltd (Shanghai, China), respectively. All animals were maintained under pathogen-free conditions. The Guide for the Care and Use of Laboratory Animals (China) conducted all experimental procedures involving animals, and the Animal Research Ethics Committee of the Sir Run Run Shaw Hospital of Zhejiang University approved the protocols.

Female C57 mice were mated with male BALB/c mice to establish an allogeneic pregnancy model (Rowe et al., 2012). The day of the vaginal plug detection was considered day 0.5 of pregnancy. SBP was measured using a noninvasive mouse tailcuff BP analyzer (BP-2010A, Softron, Japan) at 12.5, and 16.5 days of gestation. Three random urine samples were collected after day 16.5 of gestation, and UACR was measured by urinary microalbumin (CH0101060, Maccura, China). Mice were euthanized on day 18.5 of gestation.

Reduction in uterine perfusion pressure mouse model

To construct a mouse model of PE, we ligated uterine arteries in pregnant mice on day 12.5 of gestation. Briefly, after 4% chloral hydrate was intraperitoneally injected for anesthesia, bilateral incisions were made on the back of the pregnant mice, and surgical sutures were used to reduce the blood flow of the bilateral uterine arcades.

Isolation of single cells from the mouse uterus and human placenta

Uterus from pregnant mice and placentas from volunteers were washed twice with ice-cold PBS and cut into small pieces. The tissues were digested with collagenase type IV (1 mg/ml, Sigma-Aldrich, USA) and DNase I (0.01 mg/ml, Sigma-Aldrich, U.S.A) in RPMI 1640 medium (Thermo Fisher Scientific) for 40 min at 200 rpm and 37 °C. The suspensions were strained through 70-μm nylon mesh and centrifuged at 500×g for 5 minutes. Leaving the supernatants, the cell pellets from human placentas need an extra purification by Ficoll (P4350, Solarbio, China) according to the manufacturer's instructions. Human $CD4^+$ memory T cells were isolated using a Human Central and Effector Memory $CD4^+$ T Cell Isolation Kit (17865, STEMCELL, Canada).

Adoptive transferred mouse model

Endogenous macrophages or $CD4^+$ T cells were depleted by injecting PLX3397 (S7818, Selleck, USA), clodronate liposomes (40337ES08, YEASEN, China) or anti-CD4 antibody (BE0003-1, BioXcell, USA) intraperitoneally every three days starting from day 10.5 of gestation.

For the adoptive transferred mouse model, phycoerythrin-conjugated anti-mouse CD4 (12-0041-82, eBioscience, USA) and Pc5.5-conjugated anti-mouse CD44 (45-0441-82, eBioscience, USA) were used to label $CD4^+$ memory-like T cells from uterus and placentas. PE-conjugated anti-mouse CD45 (E-AB-F1136D, Elabscience, China), FITC-conjugated anti-mouse F4/80 (11-4801-82, eBioscience, USA), and PE-Cyanine7-conjugated anti-mouse CD206 (141719, Biolegend, USA) were used to label anti-inflam Macs from uterus and placentas, and the remaining $CD45^+F480^+CD206^-$ cells were considered pro-inflam Macs. The MoFlo Astrios EQ FACS Cell Sorter at Core Facilities, ZheJiang University School of Medicine (China), was used to obtain specific cells with a purity of > 96%. Briefly, 2–5 × 10^5 $CD4^+$ $CD44^+$ T cells, 5×10^5 pro-inflam Macs, or 5×10^5 anti-inflam Macs were injected to pregnant C57 mice intravenously at day 12.5 of gestation.

2–5 × 10^5 $CD45^+CD4^+$ T cells from uterus and placentas of pregnant mice were sorted

and transferred to pregnant C57 mice at day 11.5 of gestation after treating with 100nM BMS-754809 (HY10200; MedChemExpress; USA) or PBS for three days in vitro.

Mass cytometry by time of flight

Placental villi rather than chorionic plate and extraplacental membranes were used for CyToF in this study. 7×10^5 immune cells from NP (n=9), PE (n=8), GDM (n=8), GDM&PE (n=7) presented in Table 1 were washed once with 1x PBS and then stained with 100μL of 2.5 μM cisplatin (Fluidigm) for 5min on ice to exclude dead cells, and then incubated in Fc receptor blocking solution before stained with surface antibodies cocktail for 30 min on ice. Cells were washed twice with FACS buffer (1xPBS+0.5%BSA) and fixed in 200μL of intercalation solution (Maxpar Fix and Perm Buffer containing 250nM 191/193Ir, Fluidigm) overnight. After fixation, cells were washed once with FACS buffer and then perm buffer (eBioscience), stained with intracellular antibodies cocktail for 30 min on ice. Cells were washed and resuspend with deionized water, adding into 20% EQ beads (Fluidigm), acquired on a mass cytometer (Helios, Fluidigm). Additionally, all PE samples enumerated in Table 1 demonstrate a late-onset preeclampsia, with placental specimens being procured from patients more than 35 weeks of gestation and less than the 38 weeks of pregnancy.

As for data analysis, data of each sample were debarcoded from raw data using a doublet-filtering scheme with unique mass-tagged barcodes firstly. Each .fcs file generated from different batches were normalized through bead normalization method. Then we manually gate data using a FlowJo software to exclude to debris, dead cells and doublets, leaving live, single immune cells. Subsequently we applied the Phenograph clustering algorithm to all cells to partition the cells into distinct phenotypes based on marker expression levels. Cell type of each cluster according to its marker expression pattern on a heatmap of cluster vs marker was annotated. Finally, we used the dimensionality reduction algorithm t-SNE to visualize the high-dimensional data in two dimensions and show distribution of each cluster and marker expression and difference among each group or different sample type.

RNA sequencing

5×10^5 $CD45^+F4/80^+CD206^-$ pro-inflam Macs (n=3) and 5×10^5 $CD45^+F4/80^+CD206^+$ anti-inflam Macs (n=3) were isolated from the uterus and placentas of mice with RUPP and high throughput sequencing and bioinformatics analyses were conducted at Shenzhen Huada Gene Technology Service Co. Ltd.(Shenzhen, China). Only differential genes with more than two-fold change and a corrected P value less than 0.05 were considered statistically significant.

Single-cell RNA sequencing (scRNA-seq)

Mice were injected with 5×10^5 $CD45^+F4/80^+CD206^-$ pro-inflam Macs or 5×10^5 $CD45^+F4/80^+CD206^+$ anti-inflam Macs at 12.5 days of gestation and euthanized on day 18.5 of gestation. $CD45^+$ immune cells from the uterus and placenta were isolated from mice transferred pro-inflam Macs and anti-inflam Macs. scRNA-seq was conducted at PLTTECH Service Co. Ltd. (Hangzhou, China).

Firstly, the outcomes of cellular high-throughput sequencing were preserved in the FASTQ file format, facilitating a rigorous evaluation of the raw data. Subsequently, the data underwent debarcoding, enabling its alignment with the reference genome to precisely identify and sieve effective cells. This process culminated in the construction of a comprehensive gene-barcode expression matrix.For the statistical analysis and visualization of gene expression levels and

Unique Molecular Identifier (UMI) counts, we leveraged the powerful Seurat software. Furthermore, we conducted a Clustering analysis rooted in the gene-barcode expression matrix, utilizing Seurat's capabilities in conjunction with Principal Component Analysis (PCA) for dimensionality reduction. This allowed us to scale down the clustering results and visually represent them in two dimensions using either Uniform Manifold Approximation and Projection (UMAP) or t-Distributed Stochastic Neighbor Embedding (tSNE). To gain deeper insights, we performed Marker genes analysis, which hinged on the clustering outcomes. This enabled us to pinpoint the genes that significantly distinguished each subgroup, thereby identifying their characteristic genes. Additionally, we analyzed and graphically represented the varying expression levels of these genes across different groups, providing a comprehensive understanding of their differences.

Isolation of NP-EVs and PE-EVs

NP-EVs and PE-EVs were isolated and identified using our published protocols (Jiang et al., 2021; X. Liu et al., 2022). Briefly, after digesting the placental tissues from NP or PE, the suspensions were filtered through 100-μm nylon mesh and centrifugated at 3,000×g for 15 minutes. Then the supernatants were filtered with a 0.22-μm filter and centrifuged at 100,000×g for 1h at 4 °C. Then the pellets of EVs were resuspended and centrifuged at 100,000×g once again. A BCA assay kit conducted Protein quantitation of EVs (23235, Thermo Fisher Scientific). To isolate the T-EVs, 500 μg of the EVs were incubated with 1 μg placental alkaline phosphatase antibody (SC-47691, Santa Cruz Biotechnology) at 4 °C overnight, then washed in the recommended buffer (PBS containing 2% exosome-free FBS and 1 mmol/L ethylenediaminetetraacetic acid), and centrifuged at 100 000×g for 1 hour at 4 °C. After resuspended, the total EVs were sorted by EasySep Mouse PE Positive Selection Kit II (17666, STEMCELL) to collect the final NP-EVs or PE-EVs.

Induction of $CD4^+$ memory-like T cells

Macrophages were obtained after five days of culture of mononuclear cells isolated from human peripheral blood following previous protocols (X. Liu et al., 2022). NP-EVs or PE-EVs in a 50 μg/mL concentration were added to macrophages and co-cultured at 37 °C for 8 h. The human $CD4^+$ naïve T cells Isolation Kit (19555, STEMCELL, Canada) was used to isolate purified $CD4^+$ naïve T cells from human peripheral blood cells according to the manufacturer's instructions. Then, $CD4^+$ naïve T cells were co-cultured with EV-treated macrophages for six days. Flow cytometry was performed to measure the frequency of memory-like Th17 cells. For animal experiments, $CD4^+$ naïve T cells sorted from the uterus and placentas of pregnant mice were cultured with the IGF1R inhibitor BMS-754807 at a concentration of 10 μM for three days before co-cultured with macrophages.

Flow cytometry

Single immune cells from the mice uterus were obtained following the method described above. After incubation with Cell Stimulation Cocktail (00-4975-93, Invitrogen, USA) for five hours at 37 °C, cells were collected and surface staining for either phycoerythrin-conjugated anti-mouse CD4 (12-0041-82, eBioscience, USA), APC-conjugated anti-mouse CD8 (100711, BioLegend, USA), phycoerythrin-Cy5.5-conjugated anti-mouse CD44 (45-0441-82, eBioscience, USA), APC-conjugated anti-mouse CD11b (101212, BioLegend, USA), FITC-conjugated anti-mouse Gr-1 (108406, BioLegend, USA), PE-Cyanine7-conjugated anti-mouse Ly6G (E-AB-F1108H, elabscience, China) or intracellular staining for

488-conjugated anti-mouse IL-17A (506910, BioLegend, USA) was performed according to the manufacturer's instructions.

Single placental and peripheral lymphocytes and were obtained following the method described above. The Human Central and Effector Memory $CD4^+$ T cell Isolation Kit (17865, STEMCELL, Canada) was used to obtain purified memory $CD4^+$ T cells, according to the manufacturer's instructions. After incubation with Cell Stimulation Cocktail (00-4975-93, Invitrogen, USA) for five hours at 37 °C, cells were collected and surface staining for phycoerythrin-conjugated anti-human CD4 (2384240, eBioscience, USA), FITC-conjugated anti-human CD45RO (304204, BioLegend, USA), and phycoerythrin-Cy7-conjugated anti-human CCR7 (353227, BioLegend, USA) or intracellular staining for APC-conjugated anti-human IL-17A (17-7179-42, eBioscience, USA) and Foxp3 (320014, BioLegend, USA) was performed according to the manufacturer's instructions.

Immunofluorescence

Frozen sections of the placentas were permeabilized with PBS containing 0.5% Triton X-100 (PBST) for 20 min and incubated for 1 h with a blocking buffer in PBST. The sections were then incubated with anti-CD4 (sc-1176, Santa Cruz Biotechnology, China) and FITC-conjugated anti-human CD45RO (304204, BioLegend, USA) at 4 °C overnight, followed by Alexa Fluor 568-conjugated secondary antibodies (dilution: 1:200, Yeasen, China) for 1 h. The slides were counterstained with 4,6-diamidino-2-phenylindole (DAPI, 1 μg/ml; Roche, Switzerland) for 20 min. Digital images were obtained using confocal fluorescence microscopy (ZEISS LSM 800, Germany). ImageJ software was used to quantify the fluorescence intensity from immunofluorescence (IF) images.

Statistical analysis

Data were analyzed using SPSS version 20. After the Shapiro-wilk test, the data were confirmed to be non-normal distribution. Kruskal-wallis test was used to compare the results of experiments with multiple groups. Student's t-test was used to compare the results of experiments with two groups. All data are presented as mean ± SEM (*$P < 0.05$, ** $P < 0.01$, *** $P < 0.001$; NS, not significant).

Acknowledgments

The authors would like to express their heartfelt gratitude to the participants for their contributions. This work was financially supported by the National Natural Science Foundation of China (82271694, 82061160494), the "Pioneer" and "Leading Goose" R&D Program of Zhejiang (2023C03033), the Zhejiang Province Natural Science Foundation key project fund (LZ24H040002), the Zhejiang Medicine and Health Science and Technology Plan Project (2023KY800).

References

Agbaglo, E., Agbadi, P., Tetteh, J. K., Ameyaw, E. K., Adu, C., & Nutor, J. J. 2022. Trends in total fertility rate in Ghana by different inequality dimensions from 1993 to 2014. *BMC Womens Health* **22**: 49. DOI: https://doi.org/10.1186/s12905-022-01629-w, PMID: 35197037

Amador, C. A., Barrientos, V., Peña, J., Herrada, A. A., González, M., Valdés, S., Carrasco, L., Alzamora, R., Figueroa, F., Kalergis, A. M., & Michea, L. 2014. Spironolactone decreases DOCA-salt-induced organ damage by blocking the activation of T helper 17 and the

downregulation of regulatory T lymphocytes. *Hypertension* **63**: 797-803. DOI: https://doi.org/10.1161/hypertensionaha.113.02883, PMID: 24420551

Aneman, I., Pienaar, D., Suvakov, S., Simic, T. P., Garovic, V. D., & McClements, L. 2020. Mechanisms of Key Innate Immune Cells in Early- and Late-Onset Preeclampsia. *Front Immunol* **11**: 1864. DOI: https://doi.org/10.3389/fimmu.2020.01864, PMID: 33013837

Bachmayer, N., Rafik Hamad, R., Liszka, L., Bremme, K., & Sverremark-Ekström, E. 2006. Aberrant uterine natural killer (NK)-cell expression and altered placental and serum levels of the NK-cell promoting cytokine interleukin-12 in pre-eclampsia. *Am J Reprod Immunol* **56**: 292-301. DOI: https://doi.org/10.1111/j.1600-0897.2006.00429.x, PMID: 17076673

Bekkering, S., Arts, R. J. W., Novakovic, B., Kourtzelis, I., van der Heijden, C., Li, Y., Popa, C. D., Ter Horst, R., van Tuijl, J., Netea-Maier, R. T., van de Veerdonk, F. L., Chavakis, T., Joosten, L. A. B., van der Meer, J. W. M., Stunnenberg, H., Riksen, N. P., & Netea, M. G. 2018. Metabolic Induction of Trained Immunity through the Mevalonate Pathway. *Cell* **172**: 135-146.e139. DOI: https://doi.org/10.1016/j.cell.2017.11.025, PMID: 29328908

Bernardes, T. P., Mol, B. W., Ravelli, A. C. J., van den Berg, P. P., Boezen, H. M., & Groen, H. 2019. Recurrence risk of preeclampsia in a linked population-based cohort: Effects of first pregnancy maximum diastolic blood pressure and gestational age. *Pregnancy Hypertens* **15**: 32-36. DOI: https://doi.org/10.1016/j.preghy.2018.10.010, PMID: 30825924

Burton, G. J., Redman, C. W., Roberts, J. M., & Moffett, A. 2019. Pre-eclampsia: pathophysiology and clinical implications. *Bmj* **366**: l2381. DOI: https://doi.org/10.1136/bmj.l2381, PMID: 31307997

Care, A. S., Bourque, S. L., Morton, J. S., Hjartarson, E. P., Robertson, S. A., & Davidge, S. T. 2018. Reduction in Regulatory T Cells in Early Pregnancy Causes Uterine Artery Dysfunction in Mice. *Hypertension* **72**: 177-187. DOI: https://doi.org/10.1161/hypertensionaha.118.10858, PMID: 29785960

Chappell, L. C., Cluver, C. A., Kingdom, J., & Tong, S. 2021. Pre-eclampsia. *Lancet* **398**: 341-354. DOI: https://doi.org/10.1016/s0140-6736(20)32335-7, PMID: 34051884

Chatterjee, P., Chiasson, V. L., Seerangan, G., De Guzman, E., Milad, M., Bounds, K. R., Gasheva, O., Tobin, R. P., Hatahet, M., Kopriva, S., Jones, K. A., Newell-Rogers, M. K., & Mitchell, B. M. 2017. Depletion of MHC class II invariant chain peptide or γ-δ T-cells ameliorates experimental preeclampsia. *Clin Sci (Lond)* **131**: 2047-2058. DOI: https://doi.org/10.1042/cs20171008, PMID: 28642294

Chen, B., Ye, B., Li, M., Wang, S., Li, J., Lai, Y., Yang, N., Ke, Z., & Zhang, H. 2022. TIGIT Deficiency Protects Mice From DSS-Induced Colitis by Regulating IL-17A-Producing CD4(+) Tissue-Resident Memory T Cells. *Front Immunol* **13**: 931761. DOI: https://doi.org/10.3389/fimmu.2022.931761, PMID: 35844584

Cornelius, D. C., Amaral, L. M., Harmon, A., Wallace, K., Thomas, A. J., Campbell, N., Scott, J., Herse, F., Haase, N., Moseley, J., Wallukat, G., Dechend, R., & LaMarca, B. 2015a. An increased population of regulatory T cells improves the pathophysiology of placental ischemia in a rat model of preeclampsia. *Am J Physiol Regul Integr Comp Physiol* **309**: R884-891. DOI: https://doi.org/10.1152/ajpregu.00154.2015, PMID: 26290102

Cornelius, D. C., Castillo, J., Porter, J., Amaral, L. M., Campbell, N., Paige, A., Thomas, A. J., Harmon, A., Cunningham, M. W., Jr., Wallace, K., Herse, F., Wallukat, G., Dechend, R., & LaMarca, B. 2015b. Blockade of CD40 ligand for intercellular communication reduces

hypertension, placental oxidative stress, and AT1-AA in response to adoptive transfer of CD4+ T lymphocytes from RUPP rats. *Am J Physiol Regul Integr Comp Physiol* **309**: R1243-1250. DOI: https://doi.org/10.1152/ajpregu.00273.2015, PMID: 26310940

Corrêa-Silva, S., Alencar, A. P., Moreli, J. B., Borbely, A. U., de, S. L. L., Scavone, C., Damasceno, D. C., Rudge, M. V. C., Bevilacqua, E., & Calderon, I. M. P. 2018. Hyperglycemia induces inflammatory mediators in the human chorionic villous. *Cytokine* **111**: 41-48. DOI: https://doi.org/10.1016/j.cyto.2018.07.020, PMID: 30114628

Deer, E., Herrock, O., Campbell, N., Cornelius, D., Fitzgerald, S., Amaral, L. M., & LaMarca, B. 2023. The role of immune cells and mediators in preeclampsia. *Nat Rev Nephrol* **19**: 257-270. DOI: https://doi.org/10.1038/s41581-022-00670-0, PMID: 36635411

Deer, E., Reeve, K. E., Amaral, L., Vaka, V. R., Franks, M., Campbell, N., Fitzgerald, S., Herrock, O., Ibrahim, T., Cornelius, D., & LaMarca, B. 2021. CD4+ T cells cause renal and placental mitochondrial oxidative stress as mechanisms of hypertension in response to placental ischemia. *Am J Physiol Renal Physiol* **320**: F47-f54. DOI: https://doi.org/10.1152/ajprenal.00398.2020, PMID: 33196321

Díaz, E., Cárdenas, M., Ariza, A. C., Larrea, F., & Halhali, A. 2005. Placental insulin and insulin-like growth factor I receptors in normal and preeclamptic pregnancies. *Clin Biochem* **38**: 243-247. DOI: https://doi.org/10.1016/j.clinbiochem.2004.10.013, PMID: 15708546

DiToro, D., Harbour, S. N., Bando, J. K., Benavides, G., Witte, S., Laufer, V. A., Moseley, C., Singer, J. R., Frey, B., Turner, H., Bruning, J., Darley-Usmar, V., Gao, M., Conover, C., Hatton, R. D., Frank, S., Colonna, M., & Weaver, C. T. 2020. Insulin-Like Growth Factors Are Key Regulators of T Helper 17 Regulatory T Cell Balance in Autoimmunity. *Immunity* **52**: 650-667.e610. DOI: https://doi.org/10.1016/j.immuni.2020.03.013, PMID: 32294406

Eghbal-Fard, S., Yousefi, M., Heydarlou, H., Ahmadi, M., Taghavi, S., Movasaghpour, A., Jadidi-Niaragh, F., Yousefi, B., Dolati, S., Hojjat-Farsangi, M., Rikhtegar, R., Nouri, M., & Aghebati-Maleki, L. 2019. The imbalance of Th17/Treg axis involved in the pathogenesis of preeclampsia. *J Cell Physiol* **234**: 5106-5116. DOI: https://doi.org/10.1002/jcp.27315, PMID: 30277561

Faas, M. M., Spaans, F., & De Vos, P. 2014. Monocytes and macrophages in pregnancy and pre-eclampsia. *Front Immunol* **5**: 298. DOI: https://doi.org/10.3389/fimmu.2014.00298, PMID: 25071761

Fanelli, G., Romano, M., Nova-Lamperti, E., Werner Sunderland, M., Nerviani, A., Scottà, C., Bombardieri, M., Quezada, S. A., Sacks, S. H., Noelle, R. J., Pitzalis, C., Lechler, R. I., Lombardi, G., & Becker, P. D. 2021. PD-L1 signaling on human memory CD4+ T cells induces a regulatory phenotype. *PLoS Biol* **19**: e3001199. DOI: https://doi.org/10.1371/journal.pbio.3001199, PMID: 33901179

Fu, B., Li, X., Sun, R., Tong, X., Ling, B., Tian, Z., & Wei, H. 2013. Natural killer cells promote immune tolerance by regulating inflammatory TH17 cells at the human maternal-fetal interface. *Proc Natl Acad Sci U S A* **110**: E231-240. DOI: https://doi.org/10.1073/pnas.1206322110, PMID: 23271808

Fu, B., Tian, Z., & Wei, H. 2014. TH17 cells in human recurrent pregnancy loss and pre-eclampsia. *Cell Mol Immunol* **11**: 564-570. DOI: https://doi.org/10.1038/cmi.2014.54, PMID: 25027967

Fukui, A., Funamizu, A., Yokota, M., Yamada, K., Nakamua, R., Fukuhara, R., Kimura, H., & Mizunuma, H. 2011. Uterine and circulating natural killer cells and their roles in women with recurrent pregnancy loss, implantation failure and preeclampsia. *J Reprod Immunol* **90**: 105-110. DOI: https://doi.org/10.1016/j.jri.2011.04.006, PMID: 21632120

Grotegut, C. A. 2016. Prevention of preeclampsia. *J Clin Invest* **126**: 4396-4398. DOI: https://doi.org/10.1172/jci91300, PMID: 27841760

Han, X., Li, W., Li, P., Zheng, Z., Lin, B., Zhou, B., Guo, K., He, P., & Yang, J. 2021. Stimulation of α7 Nicotinic Acetylcholine Receptor by Nicotine Suppresses Decidual M1 Macrophage Polarization Against Inflammation in Lipopolysaccharide-Induced Preeclampsia-Like Mouse Model. *Front Immunol* **12**: 642071. DOI: https://doi.org/10.3389/fimmu.2021.642071, PMID: 33995360

Jensen, F., Wallukat, G., Herse, F., Budner, O., El-Mousleh, T., Costa, S. D., Dechend, R., & Zenclussen, A. C. 2012. CD19+CD5+ cells as indicators of preeclampsia. *Hypertension* **59**: 861-868. DOI: https://doi.org/10.1161/hypertensionaha.111.188276, PMID: 22353610

Jiang, L., Fei, H., Jin, X., Liu, X., Yang, C., Li, C., Chen, J., Yang, A., Zhu, J., Wang, H., Fei, X., & Zhang, S. 2021. Extracellular Vesicle-Mediated Secretion of HLA-E by Trophoblasts Maintains Pregnancy by Regulating the Metabolism of Decidual NK Cells. *Int J Biol Sci* **17**: 4377-4395. DOI: https://doi.org/10.7150/ijbs.63390, PMID: 34803505

Jung, E., Romero, R., Yeo, L., Gomez-Lopez, N., Chaemsaithong, P., Jaovisidha, A., Gotsch, F., & Erez, O. 2022. The etiology of preeclampsia. *Am J Obstet Gynecol* **226**: S844-s866. DOI: https://doi.org/10.1016/j.ajog.2021.11.1356, PMID: 35177222

Kieffer, T. E. C., Laskewitz, A., Scherjon, S. A., Faas, M. M., & Prins, J. R. 2019. Memory T Cells in Pregnancy. *Front Immunol* **10**: 625. DOI: https://doi.org/10.3389/fimmu.2019.00625, PMID: 31001255

Köstlin-Gille, N., Dietz, S., Schwarz, J., Spring, B., Pauluschke-Fröhlich, J., Poets, C. F., & Gille, C. 2019. HIF-1α-Deficiency in Myeloid Cells Leads to a Disturbed Accumulation of Myeloid Derived Suppressor Cells (MDSC) During Pregnancy and to an Increased Abortion Rate in Mice. *Front Immunol* **10**: 161. DOI: https://doi.org/10.3389/fimmu.2019.00161, PMID: 30804946

Lager, S., Sovio, U., Eddershaw, E., van der Linden, M. W., Yazar, C., Cook, E., Happerfield, L., Jessop, F. A., Sebire, N. J., Charnock-Jones, D. S., & Smith, G. C. S. 2020. Abnormal placental CD8(+) T-cell infiltration is a feature of fetal growth restriction and pre-eclampsia. *J Physiol* **598**: 5555-5571. DOI: https://doi.org/10.1113/jp279532, PMID: 32886802

LaMarca, B., Wallace, K., Herse, F., Wallukat, G., Martin, J. N., Jr., Weimer, A., & Dechend, R. 2011. Hypertension in response to placental ischemia during pregnancy: role of B lymphocytes. *Hypertension* **57**: 865-871. DOI: https://doi.org/10.1161/hypertensionaha.110.167569, PMID: 21357287

Lampé, R., Kövér, Á., Szűcs, S., Pál, L., Árnyas, E., Ádány, R., & Póka, R. 2015. Phagocytic index of neutrophil granulocytes and monocytes in healthy and preeclamptic pregnancy. *J Reprod Immunol* **107**: 26-30. DOI: https://doi.org/10.1016/j.jri.2014.11.001, PMID: 25534923

Lampé, R., Szucs, S., Adány, R., & Póka, R. 2011. Granulocyte superoxide anion production and regulation by plasma factors in normal and preeclamptic pregnancy. *J Reprod Immunol* **89**: 199-206. DOI: https://doi.org/10.1016/j.jri.2011.01.019, PMID: 21529965

Lang, X., Liu, W., Hou, Y., Zhao, W., Yang, X., Chen, L., Yan, Q., & Cheng, W. 2021. IL-17A polymorphism (rs2275913) and levels are associated with preeclampsia pathogenesis in Chinese patients. *BMC Med Genomics* **14**: 5. DOI: https://doi.org/10.1186/s12920-020-00840-8, PMID: 33407460

Lewis, E. L., Sierra, L. J., Barila, G. O., Brown, A. G., Porrett, P. M., & Elovitz, M. A. 2018. Placental immune state shifts with gestational age. *Am J Reprod Immunol* **79**: e12848. DOI: https://doi.org/10.1111/aji.12848, PMID: 29577513

Li, M., Sun, F., Xu, Y., Chen, L., Chen, C., Cui, L., Qian, J., Li, D., Wang, S., & Du, M. 2022. Tim-3(+) decidual Mφs induced Th2 and Treg bias in decidual CD4(+)T cells and promoted pregnancy maintenance via CD132. *Cell Death Dis* **13**: 454. DOI: https://doi.org/10.1038/s41419-022-04899-2, PMID: 35550500

Liao, G., Cheng, D., Li, J., & Hu, S. 2021. Clinical significance of microRNA-320a and insulin-like growth factor-1 receptor in early-onset preeclampsia patients. *Eur J Obstet Gynecol Reprod Biol* **263**: 164-170. DOI: https://doi.org/10.1016/j.ejogrb.2021.06.032, PMID: 34218203

Lisonkova, S., & Joseph, K. S. 2013. Incidence of preeclampsia: risk factors and outcomes associated with early- versus late-onset disease. *Am J Obstet Gynecol* **209**: 544.e541-544.e512. DOI: https://doi.org/10.1016/j.ajog.2013.08.019, PMID: 23973398

Liu, D., Li, Q., Ding, H., Zhao, G., Wang, Z., Cao, C., Dai, Y., Zheng, M., Zhu, X., Wu, Q., Wang, Y., Duan, H., Tang, H., Lu, X., Hou, Y., & Hu, Y. 2021. Placenta-derived IL-32β activates neutrophils to promote preeclampsia development. *Cell Mol Immunol* **18**: 979-991. DOI: https://doi.org/10.1038/s41423-021-00636-5, PMID: 33707686

Liu, X., Fei, H., Yang, C., Wang, J., Zhu, X., Yang, A., Shi, Z., Jin, X., Yang, F., Wu, D., Jiang, L., & Zhang, S. 2022. Trophoblast-Derived Extracellular Vesicles Promote Preeclampsia by Regulating Macrophage Polarization. *Hypertension* **79**: 2274-2287. DOI: https://doi.org/10.1161/hypertensionaha.122.19244, PMID: 35993233

Lu, D., Peng, Q., Chen, D., Chen, X., & Jiang, M. 2020. Expression imbalance of IL-17/IL-35 in peripheral blood and placental tissue of pregnant women in preeclampsia. *Taiwan J Obstet Gynecol* **59**: 409-414. DOI: https://doi.org/10.1016/j.tjog.2020.03.013, PMID: 32416889

Madhur, M. S., Elijovich, F., Alexander, M. R., Pitzer, A., Ishimwe, J., Van Beusecum, J. P., Patrick, D. M., Smart, C. D., Kleyman, T. R., Kingery, J., Peck, R. N., Laffer, C. L., & Kirabo, A. 2021. Hypertension: Do Inflammation and Immunity Hold the Key to Solving this Epidemic? *Circ Res* **128**: 908-933. DOI: https://doi.org/10.1161/circresaha.121.318052, PMID: 33793336

McElwain, C. J., McCarthy, F. P., & McCarthy, C. M. 2021. Gestational Diabetes Mellitus and Maternal Immune Dysregulation: What We Know So Far. *Int J Mol Sci* **22**. DOI: https://doi.org/10.3390/ijms22084261, PMID: 33923959

McIntyre, H. D., Catalano, P., Zhang, C., Desoye, G., Mathiesen, E. R., & Damm, P. 2019. Gestational diabetes mellitus. *Nat Rev Dis Primers* **5**: 47. DOI: https://doi.org/10.1038/s41572-019-0098-8, PMID: 31296866

Miller, D., Garcia-Flores, V., Romero, R., Galaz, J., Pique-Regi, R., & Gomez-Lopez, N. 2022. Single-Cell Immunobiology of the Maternal-Fetal Interface. *J Immunol* **209**: 1450-1464. DOI: https://doi.org/10.4049/jimmunol.2200433, PMID: 36192116

Morita, K., Tsuda, S., Kobayashi, E., Hamana, H., Tsuda, K., Shima, T., Nakashima, A., Ushijima, A., Kishi, H., & Saito, S. 2020. Analysis of TCR Repertoire and PD-1 Expression in Decidual and Peripheral CD8(+) T Cells Reveals Distinct Immune Mechanisms in Miscarriage and Preeclampsia. *Front Immunol* **11**: 1082. DOI: https://doi.org/10.3389/fimmu.2020.01082, PMID: 32582176

Nerenberg, K. A., Johnson, J. A., Leung, B., Savu, A., Ryan, E. A., Chik, C. L., & Kaul, P. 2013. Risks of gestational diabetes and preeclampsia over the last decade in a cohort of Alberta women. *J Obstet Gynaecol Can* **35**: 986-994. DOI: https://doi.org/10.1016/s1701-2163(15)30786-6, PMID: 24246398

Novotny, S. R., Wallace, K., Heath, J., Moseley, J., Dhillon, P., Weimer, A., Wallukat, G., Herse, F., Wenzel, K., Martin, J. N., Jr., Dechend, R., & Lamarca, B. 2012. Activating autoantibodies to the angiotensin II type I receptor play an important role in mediating hypertension in response to adoptive transfer of CD4+ T lymphocytes from placental ischemic rats. *Am J Physiol Regul Integr Comp Physiol* **302**: R1197-1201. DOI: https://doi.org/10.1152/ajpregu.00623.2011, PMID: 22461177

Ostlund, I., Haglund, B., & Hanson, U. 2004. Gestational diabetes and preeclampsia. *Eur J Obstet Gynecol Reprod Biol* **113**: 12-16. DOI: https://doi.org/10.1016/j.ejogrb.2003.07.001, PMID: 15036703

Rasmussen, T. A., Zerbato, J. M., Rhodes, A., Tumpach, C., Dantanarayana, A., McMahon, J. H., Lau, J. S. Y., Chang, J. J., Gubser, C., Brown, W., Hoh, R., Krone, M., Pascoe, R., Chiu, C. Y., Bramhall, M., Lee, H. J., Haque, A., Fromentin, R., Chomont, N., Milush, J., et al. 2022. Memory CD4(+) T cells that co-express PD1 and CTLA4 have reduced response to activating stimuli facilitating HIV latency. *Cell Rep Med* **3**: 100766. DOI: https://doi.org/10.1016/j.xcrm.2022.100766, PMID: 36198308

Robajac, D., Masnikosa, R., Miković, Ž., Mandić, V., & Nedić, O. 2015. Oxidation of placental insulin and insulin-like growth factor receptors in mothers with diabetes mellitus or preeclampsia complicated with intrauterine growth restriction. *Free Radic Res* **49**: 984-989. DOI: https://doi.org/10.3109/10715762.2015.1020798, PMID: 25812587

Rowe, J. H., Ertelt, J. M., Xin, L., & Way, S. S. 2012. Pregnancy imprints regulatory memory that sustains anergy to fetal antigen. *Nature* **490**: 102-106. DOI: https://doi.org/10.1038/nature11462, PMID: 23023128

Saito, S., Shiozaki, A., Nakashima, A., Sakai, M., & Sasaki, Y. 2007. The role of the immune system in preeclampsia. *Mol Aspects Med* **28**: 192-209. DOI: https://doi.org/10.1016/j.mam.2007.02.006, PMID: 17433431

Santner-Nanan, B., Peek, M. J., Khanam, R., Richarts, L., Zhu, E., Fazekas de St Groth, B., & Nanan, R. 2009. Systemic increase in the ratio between Foxp3+ and IL-17-producing CD4+ T cells in healthy pregnancy but not in preeclampsia. *J Immunol* **183**: 7023-7030. DOI: https://doi.org/10.4049/jimmunol.0901154, PMID: 19915051

Sasaki, Y., Darmochwal-Kolarz, D., Suzuki, D., Sakai, M., Ito, M., Shima, T., Shiozaki, A., Rolinski, J., & Saito, S. 2007. Proportion of peripheral blood and decidual CD4(+) CD25(bright) regulatory T cells in pre-eclampsia. *Clin Exp Immunol* **149**: 139-145. DOI: https://doi.org/10.1111/j.1365-2249.2007.03397.x, PMID: 17459078

Schneider, S., Freerksen, N., Röhrig, S., Hoeft, B., & Maul, H. 2012. Gestational diabetes and preeclampsia--similar risk factor profiles? *Early Hum Dev* **88**: 179-184. DOI:

https://doi.org/10.1016/j.earlhumdev.2011.08.004, PMID: 21890288

Schonkeren, D., van der Hoorn, M. L., Khedoe, P., Swings, G., van Beelen, E., Claas, F., van Kooten, C., de Heer, E., & Scherjon, S. 2011. Differential distribution and phenotype of decidual macrophages in preeclamptic versus control pregnancies. *Am J Pathol* **178**: 709-717. DOI: https://doi.org/10.1016/j.ajpath.2010.10.011, PMID: 21281803

Shields, C. A., McCalmon, M., Ibrahim, T., White, D. L., Williams, J. M., LaMarca, B., & Cornelius, D. C. 2018. Placental ischemia-stimulated T-helper 17 cells induce preeclampsia-associated cytolytic natural killer cells during pregnancy. *Am J Physiol Regul Integr Comp Physiol* **315**: R336-r343. DOI: https://doi.org/10.1152/ajpregu.00061.2018, PMID: 29718698

Spradley, F. T., Palei, A. C., & Granger, J. P. 2015. Immune Mechanisms Linking Obesity and Preeclampsia. *Biomolecules* **5**: 3142-3176. DOI: https://doi.org/10.3390/biom5043142, PMID: 26569331

Travis, O. K., White, D., Baik, C., Giachelli, C., Thompson, W., Stubbs, C., Greer, M., Lemon, J. P., Williams, J. M., & Cornelius, D. C. 2020. Interleukin-17 signaling mediates cytolytic natural killer cell activation in response to placental ischemia. *Am J Physiol Regul Integr Comp Physiol* **318**: R1036-r1046. DOI: https://doi.org/10.1152/ajpregu.00285.2019, PMID: 32320265

Wallace, K., Novotny, S., Heath, J., Moseley, J., Martin, J. N., Jr., Owens, M. Y., & LaMarca, B. 2012. Hypertension in response to CD4(+) T cells from reduced uterine perfusion pregnant rats is associated with activation of the endothelin-1 system. *Am J Physiol Regul Integr Comp Physiol* **303**: R144-149. DOI: https://doi.org/10.1152/ajpregu.00049.2012, PMID: 22647295

Wang, S., Zhu, X., Xu, Y., Zhang, D., Li, Y., Tao, Y., Piao, H., Li, D., & Du, M. 2016. Programmed cell death-1 (PD-1) and T-cell immunoglobulin mucin-3 (Tim-3) regulate CD4+ T cells to induce Type 2 helper T cell (Th2) bias at the maternal-fetal interface. *Hum Reprod* **31**: 700-711. DOI: https://doi.org/10.1093/humrep/dew019, PMID: 26908841

Weissgerber, T. L., & Mudd, L. M. 2015. Preeclampsia and diabetes. *Curr Diab Rep* **15**: 9. DOI: https://doi.org/10.1007/s11892-015-0579-4, PMID: 25644816

Yao, Y., Xu, X. H., & Jin, L. 2019. Macrophage Polarization in Physiological and Pathological Pregnancy. *Front Immunol* **10**: 792. DOI: https://doi.org/10.3389/fimmu.2019.00792, PMID: 31037072

Zhong, X., Gao, W., Degauque, N., Bai, C., Lu, Y., Kenny, J., Oukka, M., Strom, T. B., & Rothstein, T. L. 2007. Reciprocal generation of Th1/Th17 and T(reg) cells by B1 and B2 B cells. *Eur J Immunol* **37**: 2400-2404. DOI: https://doi.org/10.1002/eji.200737296, PMID: 17683116

Zhou, J., Nefedova, Y., Lei, A., & Gabrilovich, D. 2018. Neutrophils and PMN-MDSC: Their biological role and interaction with stromal cells. *Semin Immunol* **35**: 19-28. DOI: https://doi.org/10.1016/j.smim.2017.12.004, PMID: 29254756

Chen,X. , Maria ,F., Melissa,M., Jasmin,H., Igor,S., Ekaterina,A., Chanung,W., Xin,B., Mary.B.F., Hu,H., Irina,S., Kim,M.W. , Carla, M. , Jonathan,K., Maxim,N., Jason, D., David,M. 2023. Microglia-mediated T cell infiltration drives neurodegeneration in tauopathy.*Nature.*615(7953):668-677.doi:10.1038/s41586-023-05788-0,PMID: 36890231.

Chen,J., Yang,J., Wang, W., Guo, D., Zhang, C., Wang,S., Lu, X., Huang,X., Wang,P., Zhang,G., Zhang,J., Wang,J., Cai,Z. 2022. Tumor extracellular vesicles mediate anti-PD-L1 therapy resistance by decoying anti-PD-L1. Cell Mol Immunol. 19(11):1290-1301. doi: 10.1038/s41423-022-00926-6, PMID: 36220994.

Nalio Ramos R, Missolo-Koussou Y, Gerber-Ferder Y, Bromley CP, Bugatti M, Núñez NG, Tosello Boari J, Richer W, Menger L, Denizeau J, Sedlik C, Caudana P, Kotsias F, Niborski LL, Viel S, Bohec M, Lameiras S, Baulande S, Lesage L, Nicolas A, Meseure D, Vincent-Salomon A, Reyal F, Dutertre CA, Ginhoux F, Vimeux L, Donnadieu E, Buttard B, Galon J, Zelenay S, Vermi W, Guermonprez P, Piaggio E, Helft J. 2022. Tissue-resident FOLR2+ macrophages associate with CD8+ T cell infiltration in human breast cancer. Cell. 2022 Mar 31;185(7):1189-1207.e25. doi: 10.1016/j.cell.2022.02.021, PMID: 35325594.

Thomas JR, Appios A, Zhao X, Dutkiewicz R, Donde M, Lee CYC, Naidu P, Lee C, Cerveira J, Liu B, Ginhoux F, Burton G, Hamilton RS, Moffett A, Sharkey A, McGovern N. 2021. Phenotypic and functional characterization of first-trimester human placental macrophages, Hofbauer cells. J Exp Med. 2021 Jan 4;218(1):e20200891. doi: 10.1084/jem.20200891.PMID: 33075123.

Che LH, Liu JW, Huo JP, Luo R, Xu RM, He C, Li YQ, Zhou AJ, Huang P, Chen YY, Ni W, Zhou YX, Liu YY, Li HY, Zhou R, Mo H, Li JM. A single-cell atlas of liver metastases of colorectal cancer reveals reprogramming of the tumor microenvironment in response to preoperative chemotherapy.Cell Discov. 2021 Sep 7;7(1):80. doi: 10.1038/s41421-021-00312-y. PMID: 34489408.

Desrumaux C, Lemaire-Ewing S, Ogier N, Yessoufou A, Hammann A, Sequeira-Le Grand A, Deckert V, Pais de Barros JP, Le Guern N, Guy J, Khan NA, Lagrost L. Plasma phospholipid transfer protein (PLTP) modulates adaptive immune functions through alternation of T helper cell polarization. Cell Mol Immunol. 2016 Nov;13(6):795-804. doi: 10.1038/cmi.2015.75. Epub 2015 Aug 31. PMID: 26320740.

He J, Song Y, Li G, Xiao P, Liu Y, Xue Y, Cao Q, Tu X, Pan T, Jiang Z, Cao X, Lai L, Wang Q. Fbxw7 increases CCL2/7 in CX3CR1hi macrophages to promote intestinal inflammation. J Clin Invest. 2019 Jun 27;129(9):3877-3893. doi: 10.1172/JCI123374.PMID: 31246581.

Wu Y, Wu C, Shi T, Cai Q, Wang T, Xiong Y, Zhang Y, Jiang W, Lu M, Chen Z, Chen J, Wang J, He R. FAP expression in adipose tissue macrophages promotes obesity and metabolic inflammation. Proc Natl Acad Sci U S A. 2023 Dec 19;120(51):e2303075120. doi: 10.1073/pnas.2303075120. Epub 2023 Dec 15. PMID: 38100414.

Jin G, Guo N, Liu Y, Zhang L, Chen L, Dong T, Liu W, Zhang X, Jiang Y, Lv G, Zhao F, Liu W, Hei Z, Yang Y, Ou J. 5-aminolevulinate and CHIL3/CHI3L1 treatment amid ischemia aids liver metabolism and reduces ischemia-reperfusion injury. Theranostics. 2023 Aug 28;13(14):4802-4820. doi: 10.7150/thno.83163. eCollection 2023. PMID: 37771779.

Nugteren S, Samsom JN. Secretory Leukocyte Protease Inhibitor (SLPI) in mucosal tissues: Protects against inflammation, but promotes cancer. Cytokine Growth Factor Rev. 2021 Jun;59:22-35. doi: 10.1016/j.cytogfr.2021.01.005. Epub 2021 Feb 10. PMID: 33602652.

Li R, Ferdinand JR, Loudon KW, Bowyer GS, Laidlaw S, Muyas F, Mamanova L, Neves JB, Bolt L, Fasouli ES, Lawson ARJ, Young MD, Hooks Y, Oliver TRW, Butler TM, Armitage JN, Aho T, Riddick ACP, Gnanapragasam V, Welsh SJ, Meyer KB, Warren AY, Tran MGB, Stewart GD, Cortés-Ciriano I, Behjati S, Clatworthy MR, Campbell PJ, Teichmann SA,

Mitchell TJ. Mapping single-cell transcriptomes in the intra-tumoral and associated territories of kidney cancer. Cancer Cell. 2022 Dec 12;40(12):1583-1599.e10. doi: 10.1016/j.ccell.2022.11.001. Epub 2022 Nov 23.PMID: 36423636.

Che LH, Liu JW, Huo JP, Luo R, Xu RM, He C, Li YQ, Zhou AJ, Huang P, Chen YY, Ni W, Zhou YX, Liu YY, Li HY, Zhou R, Mo H, Li JM. A single-cell atlas of liver metastases of colorectal cancer reveals reprogramming of the tumor microenvironment in response to preoperative chemotherapy. Cell Discov. 2021 Sep 7;7(1):80. doi: 10.1038/s41421-021-00312-y.PMID: 34489408.

Coppo L, Mishra P, Siefert N, Holmgren A, Pääbo S, Zeberg H. A substitution in the glutathione reductase lowers electron leakage and inflammation in modern humans. Sci Adv. 2022 Jan 7;8(1):eabm1148. doi: 10.1126/sciadv.abm1148. Epub 2022 Jan 5. PMID: 34985944.

Hang S, Paik D, Yao L, Kim E, Trinath J, Lu J, Ha S, Nelson BN, Kelly SP, Wu L, Zheng Y, Longman RS, Rastinejad F, Devlin AS, Krout MR, Fischbach MA, Littman DR, Huh JR. Bile acid metabolites control TH17 and Treg cell differentiation.Nature. 2019 Dec;576(7785):143-148. doi: 10.1038/s41586-019-1785-z. Epub 2019 Nov 27. PMID: 31776512.

Leite JA, Menezes L, Martins E, Rodrigues TS, Tavares L, Ebering A, Schelmbauer C, Martelossi Cebinelli GC, Zinina V, Golden A, Soshnikova N, Zamboni DS, Cunha FQ, Huber M, Silva JS, Waisman A, Carlos D, Saraiva Câmara NO. AIM2 promotes TH17 cells differentiation by regulating RORγt transcription activity. iScience. 2023 Oct 4;26(11):108134. doi: 10.1016/j.isci.2023.108134. eCollection 2023 Nov 17. PMID: 37867943.

Evrard M, Becht E, Fonseca R, Obers A, Park SL, Ghabdan-Zanluqui N, Schroeder J, Christo SN, Schienstock D, Lai J, Burn TN, Clatch A, House IG, Beavis P, Kallies A, Ginhoux F, Mueller SN, Gottardo R, Newell EW, Mackay LK. Single-cell protein expression profiling resolves circulating and resident memory T cell diversity across tissues and infection contexts. Immunity. 2023 Jul 11;56(7):1664-1680.e9. doi: 10.1016/j.immuni.2023.06.005. Epub 2023 Jun 30. PMID: 37392736.

Bieberich F, Vazquez-Lombardi R, Yermanos A, Ehling RA, Mason DM, Wagner B, Kapetanovic E, Di Roberto RB, Weber CR, Savic M, Rudolf F, Reddy ST. A Single-Cell Atlas of Lymphocyte Adaptive Immune Repertoires and Transcriptomes Reveals Age-Related Differences in Convalescent COVID-19 Patients. Front Immunol. 2021 Jul 12;12:701085. doi: 10.3389/fimmu.2021.701085. eCollection 2021. PMID: 34322127.

Qiu C, Du G. Loss of LEF-1 expression as a diagnostic indicator for extranodal NK/T-cell lymphoma: An immunohistochemical study of 88 cases. Eur J Haematol. 2022 Nov;109(5):513-518. doi: 10.1111/ejh.13836. Epub 2022 Aug 2.PMID: 35871391.

Sekine T, Perez-Potti A, Nguyen S, Gorin JB, Wu VH, Gostick E, Llewellyn-Lacey S, Hammer Q, Falck-Jones S, Vangeti S, Yu M, Smed-Sörensen A, Gaballa A, Uhlin M, Sandberg JK, Brander C, Nowak P, Goepfert PA, Price DA, Betts MR, Buggert M. TOX is expressed by exhausted and polyfunctional human effector memory CD8+ T cells. Sci Immunol. 2020 Jul 3;5(49):eaba7918. doi: 10.1126/sciimmunol.aba7918. PMID: 32620560.

Esensten JH, Helou YA, Chopra G, Weiss A, Bluestone JA. CD28 Costimulation: From Mechanism to Therapy. Immunity. 2016 May 17;44(5):973-88. doi:10.1016/j.immuni.2016.04.020. PMID: 27192564.

Pai JA, Hellmann MD, Sauter JL, Mattar M, Rizvi H, Woo HJ, Shah N, Nguyen EM, Uddin FZ, Quintanal-Villalonga A, Chan JM, Manoj P, Allaj V, Baine MK, Bhanot UK, Jain M, Linkov I, Meng F, Brown D, Chaft JE, Plodkowski AJ, Gigoux M, Won HH, Sen T, Wells DK, Donoghue MTA, de Stanchina E, Wolchok JD, Loomis B, Merghoub T, Rudin CM, Chow A, Satpathy AT. Lineage tracing reveals clonal progenitors and long-term persistence of tumor-specific T cells during immune checkpoint blockade. Cancer Cell. 2023 Apr 10;41(4):776-790.e7. doi: 10.1016/j.ccell.2023.03.009. Epub 2023 Mar 30. PMID: 37001526.

Montaldo E, Lusito E, Bianchessi V, Caronni N, Scala S, Basso-Ricci L, Cantaffa C, Masserdotti A, Barilaro M, Barresi S, Genua M, Vittoria FM, Barbiera G, Lazarevic D, Messina C, Xue E, Marktel S, Tresoldi C, Milani R, Ronchi P, Gattillo S, Santoleri L, Di Micco R, Ditadi A, Belfiori G, Aleotti F, Naldini MM, Gentner B, Gardiman E, Tamassia N, Cassatella MA, Hidalgo A, Kwok I, Ng LG, Crippa S, Falconi M, Pettinella F, Scapini P, Naldini L, Ciceri F, Aiuti A, Ostuni R. Cellular and transcriptional dynamics of human neutrophils at steady state and upon stress. Nat Immunol. 2022 Oct;23(10):1470-1483. doi: 10.1038/s41590-022-01311-1. Epub 2022 Sep 22.PMID: 36138183.

Wenzel P, Rossmann H, Müller C, Kossmann S, Oelze M, Schulz A, Arnold N, Simsek C, Lagrange J, Klemz R, Schönfelder T, Brandt M, Karbach SH, Knorr M, Finger S, Neukirch C, Häuser F, Beutel ME, Kröller-Schön S, Schulz E, Schnabel RB, Lackner K, Wild PS, Zeller T, Daiber A, Blankenberg S, Münzel T. Heme oxygenase-1 suppresses a pro-inflammatory phenotype in monocytes and determines endothelial function and arterial hypertension in mice and humans. Eur Heart J. 2015 Dec 21;36(48):3437-46. doi: 10.1093/eurheartj/ehv544. Epub 2015 Oct 29. PMID: 26516175.

Ulff-Møller CJ, Asmar F, Liu Y, Svendsen AJ, Busato F, Grønbaek K, Tost J, Jacobsen S. Twin DNA Methylation Profiling Reveals Flare-Dependent Interferon Signature and B Cell Promoter Hypermethylation in Systemic Lupus Erythematosus. Arthritis Rheumatol. 2018 Jun;70(6):878-890. doi: 10.1002/art.40422. Epub 2018 May 9. PMID: 29361205.

Drummond RA, Swamydas M, Oikonomou V, Zhai B, Dambuza IM, Schaefer BC, Bohrer AC, Mayer-Barber KD, Lira SA, Iwakura Y, Filler SG, Brown GD, Hube B, Naglik JR, Hohl TM, Lionakis MS. CARD9+ microglia promote antifungal immunity via IL-1β- and CXCL1-mediated neutrophil recruitment. Nat Immunol. 2019 May;20(5):559-570. doi: 10.1038/s41590-019-0377-2. Epub 2019 Apr 17. PMID: 30996332.

von Wulffen M, Luehrmann V, Robeck S, Russo A, Fischer-Riepe L, van den Bosch M, van Lent P, Loser K, Gabrilovich DI, Hermann S, Roth J, Vogl T. S100A8/A9-alarmin promotes local myeloid-derived suppressor cell activation restricting severe autoimmune arthritis. Cell Rep. 2023 Aug 29;42(8):113006. doi: 10.1016/j.celrep.2023.113006. Epub 2023 Aug 22. PMID: 37610870.

Kao KD, Grasberger H, El-Zaatari M. The Cxcr2+ subset of the S100a8+ gastric granylocytic myeloid-derived suppressor cell population (G-MDSC) regulates gastric pathology. Front Immunol. 2023 Sep 8;14:1147695. doi: 10.3389/fimmu.2023.1147695. eCollection 2023. PMID: 37744359.

Robertson SA, Green ES, Care AS, Moldenhauer LM, Prins JR, Hull ML, Barry SC, Dekker G. Therapeutic Potential of Regulatory T Cells in Preeclampsia-Opportunities and Challenges. Front Immunol. 2019 Mar 21;10:478. doi: 10.3389/fimmu.2019.00478. eCollection 2019. PMID: 30984163

Sefik E, Geva-Zatorsky N, Oh S, Konnikova L, Zemmour D, McGuire AM, Burzyn D, Ortiz-Lopez A, Lobera M, Yang J, Ghosh S, Earl A, Snapper SB, Jupp R, Kasper D, Mathis D, Benoist C. MUCOSAL IMMUNOLOGY. Individual intestinal symbionts induce a distinct population of RORγ□ regulatory T cells. Science. 2015 Aug 28;349(6251):993-7. doi: 10.1126/science.aaa9420. Epub 2015 Aug 13. PMID: 26272906

Akkari L, Amit I, Bronte V, Fridlender ZG, Gabrilovich DI, Ginhoux F, Hedrick CC, Ostrand-Rosenberg S. Defining myeloid-derived suppressor cells. Nat Rev Immunol. 2024 Jul 5. doi: 10.1038/s41577-024-01062-0. Online ahead of print. PMID: 38969773

Aneman I, Pienaar D, Suvakov S, Simic TP, Garovic VD, McClements L.Mechanisms of Key Innate Immune Cells in Early- and Late-Onset Preeclampsia.Front Immunol. 2020 Aug 18;11:1864. doi: 10.3389/fimmu.2020.01864. eCollection 2020. PMID: 33013837

Luo F, Liu F, Guo Y, Xu W, Li Y, Yi J, Fournier T, Degrelle S, Zitouni H, Hernandez I, Liu X, Huang Y, Yue J.Single-cell profiling reveals immune disturbances landscape and HLA-F-mediated immune tolerance at the maternal-fetal interface in preeclampsia.Front Immunol. 2023 Oct 3;14:1234577. doi: 10.3389/fimmu.2023.1234577. eCollection 2023.PMID: 37854606

Li Y, Sang Y, Chang Y, Xu C, Lin Y, Zhang Y, Chiu PCN, Yeung WSB, Zhou H, Dong N, Xu L, Chen J, Zhao W, Liu L, Yu D, Zang X, Ye J, Yang J, Wu Q, Li D, Wu L, Du M. A Galectin-9-Driven CD11c^{high} Decidual Macrophage Subset Suppresses Uterine Vascular Remodeling in Preeclampsia.Circulation. 2024 May 21;149(21):1670-1688. doi:10.1161/CIRCULATIONAHA.123.064391. Epub 2024 Feb 5.PMID: 38314577

Figures with figure Legends

Figure 1 Identification and characterization of placental immune cells using CyTOF

(A) Schematic of the experimental workflow in CyTOF experiment. The placentas were obtained from individuals with normal pregnancy (NP, n=9), preeclampsia (PE, n=8), gestational diabetes mellitus (GDM, n=8) or GDM&PE (n=7).

(B) t-SNE maps showing 7×10^5 CD45$^+$ cells from the placenta overlaid with color-coded clusters and the distributions of B cells, CD4$^+$ T cells, CD8$^+$ T cells, DC, γδT cells, monocytes, granulocytes, MDSC, and NK cells.

(C) Percentages of each cell type of CD45$^+$ cells in placentas.

(D) t-SNE maps showing the expression of CD3, CD8, CD4, γδTCR, CD14, CD15, CD56.

(E) Heatmap showing the expression levels of markers in CD45$^+$ cell subsets.

Data were compared between NP and PE, NP and GDM, NP and GDM&PE using the Kruskal-wallis test and represented as mean±SEM (*P < 0.05, ** P < 0.01, *** P < 0.001; NS, not significant).

Figure 2 Specific altered T cell profile in the placentas of individuals with PE

(A) Distribution of the CD4$^+$ T cells analyzed using t-SNE.

(B) Scatter dot plots showing the frequencies of cluster 8 of $CD4^+$ T cells in the placentas of individuals with NP, PE, GDM and GDM&PE (n=9 in NP group; n=8 in PE group; n=8 in GDM group; n=7 in GDM&PE group).

(C) Expression of IL-17A and Foxp3 in $CD45RO^+CCR7^+CD4^+$ T cells in placentas of individuals with NP and PE using flow cytometry (IL-17A: n=10 in NP group, n=15 in PE group; Foxp3: n=7 in NP group, n=9 in PE group).

(D) Immunofluorescence co-staining of CD4 (red), CD45RO (green) and DAPI (blue) in frozen placental sections. The right panels show the fluorescence intensity of CD4 and CD45RO.Scale bar, 20 µm.

(E) Scatter dot plots showing significantly altered markers of in cluster 8 of $CD4^+$ T cells.

(F) Distribution of the $CD8^+$ T cells analyzed using t-SNE.

(G) Scatter dot plots showing the frequencies of cluster 2 of $CD8^+$ T cells in the placentas of individuals with NP, PE, GDM and GDM&PE.

(H) Scatter dot plots showing significantly altered markers in cluster 2 of $CD8^+$ T cells.

(I) Distribution of the γδT cells analyzed using t-SNE.

(J) Scatter dot plots showing the frequencies of cluster 15 of γδT cells in the placentas of individuals with NP, PE, GDM and GDM&PE.

(K) Scatter dot plots showing significantly altered markers in cluster 15 of γδT cells.

Data were compared between NP and PE, NP and GDM, NP and GDM&PE using the Kruskal-wallis test and represented as mean±SEM (*P < 0.05, ** P < 0.01, *** P < 0.001; NS, not significant).

Figure 2—figure supplement 1 Identification of the placental T cell subsets.

(A) Heatmap showing the expression levels of markers in the $CD4^+$ T subsets (n=9 in NP group; n=8 in PE group; n=8 in GDM group; n=7 in GDM&PE group).

(B) Heatmap showing the expression levels of markers in the $CD8^+$ T subsets.

(C) Heatmap showing the expression levels of markers in the γδT subsets.

Figure 3 Identification of the placental $CD11b^+$ cell subsets and the Interaction between placental immune cells.

(A) Distribution of the $CD11b^+$ immune cells analyzed using t-SNE.

(B) Heatmap showing the expression levels of markers in the $CD11b^+$ cells.

(C) Scatter dot plots showing the frequencies of cluster 12, cluster 23, and cluster 25 of $CD11b^+$ cells in the placentas.

(D) Interaction between placental immune cells showed in heatmap.

(E) Scatter plots of Pearson's correlation analysis between placental immune cells.

Data were compared between NP and PE, NP and GDM, NP and GDM&PE using the Kruskal-wallis test and represented as mean±SEM (*P < 0.05, ** P < 0.01, *** P < 0.001; NS, not significant).

Figure 4 The immune imbalance at the maternal-fetal interface induced by $F480^+CD206^-$ pro-inflam Macs.

(A) An illustration showcasing the RNA-seq of the $CD45^+F4/80^+CD206^-$ pro-inflam Macs and $CD45^+F4/80^+CD206^+$ anti-inflam Macs derived from the RUPP mouse model.

(B) Principal component analysis (PCA) reflected the differences between the two groups of

macrophages (n=3).

(C) The volcano map shows a comparison of the content and P value of gene expression between pro-inflam Macs and anti-inflam Macs. Differential expression genes were screened out when $P < 0.05$. Red dots indicate genes with increased expression in pro-inflam Macs. Blue dots indicate genes with decreased expression.

(D) The volcano map shows differential expression genes between pro-inflam Macs and anti-inflam Macs.

(E) Representative pathways enriched in the identified genes as determined by GSEA (p value<0.05).

(F) Embryo abortion rate of the pregnant mice, body weight and crown-rump length of pups measured on day 18.5 of gestation. Black represents mice treated with DMSO (n=8); gray represents mice treated with PLX3397 (n=8); blue represents mice injected with $CD45^+F4/80^+CD206^+$ anti-inflammatory macrophages (n=8); red represents mice injected with $CD45^+F4/80^+CD206^-$ pro-inflammatory macrophages (n=8).

(G) SBP and UACR of pregnant mice in the four groups.

(H) Frequencies of $CD44^+CD4^+IL\text{-}17A^+$ cells, $CD44^+CD8^+$ T cells and $CD11b^+Ly6G^+$ granulocytes analyzed by flow cytometry.

Data were compared between groups using the Kruskal-wallis test and represented as mean±SEM (*P < 0.05, ** P < 0.01, *** P < 0.001).

Figure 4—figure supplement 1 The construction of RUPP mouse model

(A) Experimental design of mice model with PE by reducing uterine perfusion pressure (RUPP) on day 12.5 of gestation. Mice with sham operation were considered as controls. Systolic blood pressure (SBP) and urine albumin creatine ratio (UACR) were measured on day 12.5 and 16.5 of gestation respectively. Mice were sacrificed on day 18.5 of gestation.

(B) The embryo abortion rate of pregnant mice, body weight, and crown-rump length of pups measured on day 18.5 of gestation in the Sham and RUPP group. Embryo abortion rate = number of absorbed embryos/total number of embryos. Blue represents mice in the Sham group (n=9); Red represents mice in the RUPP group (n=9).

(C) SBP and UACR of pregnant mice in Sham and RUPP group.

(D) Experimental design of GFP pregnant mice model.

(E) Frequencies of GFP^+CD11b^+ fetal-derived macrophages and GFP^-CD11b^+ maternal-derived macrophages were analyzed by flow cytometry.

Data were compared between the two groups using the Student's t-test and represented as mean±SEM (*P < 0.05, ** P < 0.01, *** P < 0.001).

Figure 4—figure supplement 2 Clodronate liposomes were used to used to deplete the macrophages of pregnant mice to demonstrate that pro-inflam Macs lead to immune imbalance.

(A) Frequencies of $F4/80^+7AAD^-$ macrophages in PLX3397-treated mouse were analyzed by flow cytometry.

(B) Frequencies of $F4/80^+7AAD^-$ macrophages in Clodronate liposomes-treated mouse were analyzed by flow cytometry.

(C) Embryo abortion rate of the pregnant mice, body weight and crown-rump length of pups measured on day 18.5 of gestation. Black represents mice treated with control liposomes (n=6); gray represents mice treated with clodronate liposomes (n=6); blue represents mice

injected with $CD45^+F4/80^+CD206^+$ anti-inflam Macs (n=6); red represents mice injected with $CD45^+F4/80^+CD206^-$ pro-inflam Macs (n=6).

(D) SBP and UACR of pregnant mice in the four groups.

(E) Frequencies of $CD44^+CD4^+IL\text{-}17A^+$ cells, $CD44^+CD8^+$ T cells and $CD11b^+Gr1^+$ granulocytes analyzed by flow cytometry.

Data were compared between groups using one-way ANOVA and represented as mean±SEM (*P < 0.05, ** P < 0.01, *** P < 0.001).

Figure 5 Identification of the macrophage subsets in mice injected with pro-inflam Macs and anti-inflam Macs by using scRNA-seq.

(A) UMAP maps showing the 8 types of mouse immune cells at the maternal-fetal interface.

(B) Heatmap showing clustering analysis for markers distinguished different type of immune cells.

(C) Heatmap showing clustering analysis for markers distinguished different clusters of macrophages.

(D) UMAP maps showing the 15 clusters of mouse macrophages was listed in the left panel. Bar graph showing the frequencies of clusters of macrophages in the two groups of mice was listed in the right panel.

(E) UMAP maps showing the distribution of specific markers of cluster 0 and cluster 1.

(F) Dot plot depicting GO enrichment terms that were significantly enriched in the differentially expressed genes in cluster 0 and cluster 1 from the pro-inflam Macs group and the control group.

(G) Violin plot of specific differential gene expression in cluster 0 and cluster 1 between the pro-inflam Macs group and the control group.

Data were compared between the two groups using the Student's t-test and represented as mean±SEM (*P < 0.05, ** P < 0.01, *** P < 0.001).

Figure 6 Identification of the T/NK cells subsets in mice injected pro-inflam Macs and anti-inflam Macs using scRNA-seq.

(A) UMAP maps showing the 12 clusters of mouse T/NK cells was listed in the up panel. Bar graph showing the frequencies of clusters of T/NK cells in the two groups of mice was listed in the down panel.

(B) Heatmap showing clustering analysis for markers distinguished 12 different clusters of T/NK cells.

(C) UMAP maps showing the distribution of specific markers of cluster 0, 1 and 2.

(D) Dot plot depicting GO enrichment terms that were significantly enriched in the differentially expressed genes in cluster 0 from the pro-inflam Macs group and the control group.

(E) Violin plot of specific differential gene expression in cluster 0 between the pro-inflam Macs group and the control group.

(F) Frequencies of $CD4^+CD44^+$ T cells and the percentages of $Foxp3^+$ or $IL\text{-}17A^+$ cells in $CD4^+CD44^+$ T cells at the maternal-fetal interface in Sham and RUPP group analyzed by flow cytometry.

(G) The embryo abortion rate of pregnant mice, body weight, and crown-rump length of pups

measured on day 18.5 of gestation in mice injected PBS, Sham mouse-derived or RUPP mouse-derived $CD4^+CD44^+$ T cells. Black represents mice injected with PBS (n=6); blue represents mice injected with Sham mouse-derived $CD4^+CD44^+$ T cells (n=6); red represents mice injected with RUPP mouse-derived $CD4^+CD44^+$ T cells (n=6).

(H) SBP and UACR of pregnant mice injected with PBS, Sham mouse-derived or RUPP mouse-derived $CD4^+CD44^+$ T cells.

Data were compared between groups using one-way ANOVA and represented as mean±SEM (*P < 0.05, ** P < 0.01, *** P < 0.001).

Data were compared between the two groups using the Student's t-test and represented as mean±SEM (*P < 0.05, ** P < 0.01, *** P < 0.001).

Figure 6—figure supplement 1 Memory-like Th17 cells may be associated with the recurrence of PE.

(A) Embryo abortion rate of pregnant mice, body weight and crown-rump length of pups measured on day 18.5 of gestation. Blue represents mice with previous normal pregnancy (n=9); red represents mice with previous pregnancy with PE (n=9).

(B) SBP and UACR of second pregnant mice with a history of PE or NP in the first pregnancy measured on day 16.5 of gestation.

(C) Frequencies of $CD4^+$ $CD44^+$ T cells and the levels of IL-17A in $CD4^+$ $CD44^+$ T cells in mice with a pregnancy history with NP and PE analyzed by flow cytometry.

Data were compared using the Student's t-test and represented as mean±SEM (*P < 0.05, ** P < 0.01, *** P < 0.001; NS, not significant).

Data were compared between the two groups using the Student's t-test and represented as mean±SEM (*P < 0.05, ** P < 0.01, *** P < 0.001).

Figure 6—figure supplement 2 Identification of the granulocytes subsets in mice injected pro-inflam Macs and anti-inflam Macs use sc RNA-seq.

(A) UMAP maps showing the 9 clusters of mouse granulocytes. Bar graph showing the frequencies of clusters of granulocytes in the two groups of mice.

(B) Heatmap showing clustering analysis for markers distinguished 9 different clusters of granulocytes cells.

(C) UMAP maps showing the distribution of specific markers of cluster 0, 1, 2 and 3.

(D) Dot plot depicting GO enrichment terms that were significantly enriched in the differentially expressed genes in cluster 3 from the pro-inflam Macs group and the control group.

(E) Violin plot of specific differential gene expression in cluster 3 between the pro-inflam Macs group and the control group.

(F) Immunofluorescence co-staining of CD15 (red), CD66b (green) and DAPI (blue) in frozen placental sections. Scale bar, 20 μm.

Data were compared between the two groups using the Student's t-test and represented as mean±SEM (*P < 0.05, ** P < 0.01, *** P < 0.001).

Figure 7 Pro-inflam Macs induce the generation of memory-like Th17 cells via IGF1-IGF1R

(A) Signaling modules indicated by ligand-receptor pairing between macrophages and other types of immune cells at the maternal-fetal interface using CellPhoneDB.

(B) Frequencies of $IGF1^+CD14^+$ cells and $IGFIR^+CD4^+$ cells in placentas of individuals with NP and PE (n=12 in NP group, n=4 in PE group).

(C) Schematic of the experimental workflow to induce memory-like T cells in vitro. Macrophages, after incubating with PBS, NP-EVs or PE-EVs, were co-cultured with $CD4^+$ naïve T cells treated with DMSO or BMS-754807. Cells were isolated from human peripheral blood.

(D) Frequencies of $CD45RO^+CCR7^+$Th17 cells. Black represents $CD4^+$ naïve T cells treated with DMSO; gray represents $CD4^+$ naïve T cells cocultured with NP-EVs-treated macrophages; blue represents $CD4^+$ naïve T cells co-cultured with PE-EVs-treated macrophages; red represents $CD4^+$ naïve T cells treated with BMS-754807 before co-cultured with PE-EVs-treated macrophages (n=10 in each group).

(E) Schematic of mice transferred $CD4^+$ T cells treated with BMS-754807 or PBS. Anti-CD4 antibody was used to deplete $CD4^+$ T cells in mice on day 10.5 of gestation. $CD4^+$ T cells were transferred into mice on day 11.5 of gestation. 20 μg/kg lipopolysaccharide (LPS) was intraperitoneally injected on day 12.5 and 15.5 of gestation to induce a PE-like pregnant mice model. Mice were sacrificed on day 18.5 of gestation.

(F) Embryo abortion rate of pregnant mice, body weight and crown-rump length of pups were measured on day 18.5 of gestation. Black represents the control group mice (n=6); gray represents mice treated with LPS (20μg/kg) to construct an animal model of PE (n=6); blue represents anti-CD4 antibody treated PE mice (n=6); red represents anti-CD4 antibody treated PE mice injected with $CD4^+$ T cells with DMSO treatment (n=7); orange represents anti-CD4 antibody treated PE mice injected with $CD4^+$ T cells with BMS754807 treatment (n=7).

(G) SBP and UACR of pregnant mice in the five groups.

(H) The frequencies of $CD4^+$ $CD44^+$ $IL\text{-}17A^+$ cells analyzed by flow cytometry.

Data were compared between groups using one-way ANOVA and represented as mean±SEM (*P < 0.05, ** P < 0.01, *** P < 0.001).

Figure 7—figure supplement 1 Cell–cell communications in immune cells when pro-inflam Macs accumulated at the maternal–fetal interface.

(A) Abundance of connections between different cell types at the maternal-fetal interface analyzed by CellPhoneDB.

(B) Capacities for interactions between immune cells are showed. Each line indicates the ligands expressed by the cell population represented by the same color (labeled). The lines connect to cell types that express cognate receptors. Line thickness is proportional to the number of ligands when cognate receptors are present in the recipient cell type.

Tables

Table 1 Details of the individuals included in the CyTOF

Parameters	NP (n=9)	PE (n=8)	GDM (n=8)	GDM&PE (n=7)	p Value
Age (years)	31.33 ± 2.108	31.75 ± 4.206	35.25 ±3.419	32.43 ± 2.321	0.1008
BMI (kg/m^2)	27.35 ± 1.740	30.84 ±2.888	29.56 ± 2.689	30.16 ± 2.280	0.0518
Gestational age (weeks)	38.89 ± 0.558	37.39 ± 1.253	38.73 ± 0.419	36.22 ± 1.372	<0.001
Number of living children	0.4444 ± 0.497	0.500 ± 0.500	1.125 ± 0.331	0.429 ± 0.495	0.0236
Previous abortions	0.7778 ± 1.030	1.000 ± 0.866	1.000 ± 1.000	1.714 ± 2.050	0.5848

Mean Systolic Blood Pressure	109.7 ± 5.400	151 ± 7.225	106.9 ± 2.848	150.7 ± 9.161	<0.0001

Table 2 CyTOF antibody panel used for analyzing placentas from individuals with normal pregnancy (NP), preeclampsia (PE), gestational diabetes mellitus (GDM) and GDM complicated with PE (GDM&PE)

Target	Metal tag
CD45	HI30
CD3	UCHT1
CD68	Y1/82A
CD56	NCAM16.2
gd TCR	5A6.E9
CD19	HIB19
CCR6	G034E3
CD38	HIT2
CD103	B-Ly7
CD39	A1
CXCR3	G025H7
PD-L1	29E.2A3
PD-1	EH12.2H7
CD11C	BU15
CD107a	H4A3
pAKT	D9E
CCR4	L291H4
TIGIT	A15153G
CD206	15-2
Helios	22F6
CD28	CD28.2
pSTAT3	4/p-Stat3
GITR	110416
CD33	WM53
CTLA-4	BN13
FOXP3	PCH101
CD163	GHI/61
CD45RA	HI100
ICOS	C398.4A
CD69	FN50
CCR7	G043H7
NKG2A	131411
CD15	W6D3
TIM-3	F38-2E2
CD86	Fun-1
HLA-DR	L243
Granzyme B	QA16A02
CD14	M5E2
pS6	A17020B
CD127	A019D5
CD4	RPA-T4
CD8	RPA-T8
CD11b	M1/70

Table 3 Expression levels of markers identified in each immune subset in the placentas

	B cells	$CD4^+$ T	$CD8^+$ T	gdTCR	NK cells	Macrophage	Granulocyte	MDSC	Dendritic cells
CD45	++	++	++	++	++	++	++	++	++
CD3	-	++	++	-	-	-	-	-	-
CD68	+	+	+	+	+	++	+	++	++
CD56	-	-	-	-	+	-	-	-	-
gd TCR	++	-	-	++	-	-	-	-	-
CD19	++	-	-	++	-	-	-	-	-
CCR6	+	-	-	-	-	-	-	-	-
CD38	++	++	+	+	++	++	-	-	+
CD103	-	-	-	-	-	-	-	-	-
CD39	++	-	-	-	+	++	+	+	+
CXCR3	+	+	+	+	+	+	-	+	++
PD-L1	-	-	-	-	-	-	-	+	-
PD-1	-	-	-	-	-	-	-	-	-
CD11C	+	-	-	-	+	++	++	+	++
CD107a	+	-	-	-	-	+	-	+	+
pAKT	+	+	+	+	+	++	+	+	+
CCR4	-	-	-	-	-	-	-	-	-
TIGIT	-	-	-	-	-	-	-	-	-
CD206	-	-	-	-	-	+	-	+	-
Helios	+	+	+	+	+	+	+	+	+
CD28	-	+	+	+	-	-	-	-	-
pSTAT3	+	+	-	+	-	+	+	-	-
GITR	-	-	-	-	-	-	-	-	-
CD33	-	-	-	-	-	+	-	+	-
CTLA-4	-	-	-	-	-	-	-	-	-
FOXP3	-	-	-	-	-	-	-	-	-
CD163	-	-	-	-	-	-	-	-	-
CD45RA	++	+	+	+	++	-	-	-	-
ICOS	-	+	+	-	-	-	-	-	-
CD69	+	+	+	+	++	+	-	++	-
CCR7	+	++	+	+	-	-	-	+	-
NKG2A	-	-	-	-	-	-	-	-	-
CD15	-	-	-	-	-	-	++	-	-
TIM-3	-	-	-	-	-	-	-	-	-
CD86	-	-	-	-	-	++	-	-	+
HLA-DR	++	-	+	+	-	++	+	-	++
Granzyme	+	-	-	+	++	+	+	-	-
CD14	-	-	-	-	-	++	-	-	-
pS6	-	-	-	-	-	-	-	-	-
CD127	-	++	+	-	-	-	-	-	-
CD4	-	++	-	-	-	-	-	-	-
CD8	-	-	++	-	-	-	-	-	-

CD11b	-	-	-	+	+	++	++	-	+

Table 4 The marker profile of PE-specific immune subsets

	memory-like $CD4^+$ T cells	memory-like $CD8^+$ T cells	gMDSCs	pro-inflammatory macrophages	anti-inflammatory macrophages
	Cluster 08 of $CD4^+$ T cells	Cluster 02 of $CD8^+$ T cells	Cluster 12 of $CD3^-CD11b^+$ cells	Cluster 23 of $CD3^-CD11b^+$ cells	Cluster 25 of $CD3^-CD11b^+$ cells
CD45	++	++	++	++	++
CD3	++	++	-	-	-
CD68	-	-	+	++	++
CD56	-	-	-	-	-
gd TCR	-	-	-	-	-
CD19	-	-	-	-	-
CCR6	-	-	-	-	-
CD38	++	++	-	+	+
CD103	-	-	-	+	+
CD39	+	-	+	-	-
CXCR3	+	+	-	-	-
PD-L1	-	-	-	-	-
PD-1	-	-	-	-	-
CD11C	-	-	++	++	++
CD107a	-	-	-	+	+
pAKT	+	+	-	-	-
CCR4	-	-	-	-	-
TIGIT	-	-	-	-	-
CD206	-	-	+	-	+
Helios	+	+	-	-	-
CD28	+	+	-	-	-
pSTAT3	-	-	-	-	-
GITR	-	-	-	-	-
CD33	-	-	-	-	+
CTLA-4	-	-	-	-	-
FOXP3	-	-	-	-	-
CD163	-	-	-	-	-
CD45RA	-	-	-	-	-
ICOS	+	+	-	-	-
CD69	+	-	-	-	-
CCR7	++	++	-	-	-
NKG2A	-	-	-	-	-
CD15	-	-	++	-	-
TIM-3	-	-	-	-	-
CD86	-	-	-	+	+
HLA-DR	-	-	+	+	++
Granzyme B	-	-	+	-	-
CD14	-	-	-	+	+
pS6	-	-	-	-	-
CD127	+	-	-	-	-
CD4	++	-	-	-	-

CD8	-	++	-	-	-
CD11b	-	-	++	++	++

Table 5 Details of the individual with NP or PE included in the study

Parameters	NP (n=30)	PE (n=30)	p Value
Age (years)	31.13 ± 2.9747	31.50 ± 4.1693	0.0741
BMI (kg/m^2)	27.24 ± 2.8048	29.48±3.9295	0.0155
Gestational age (weeks)	38.68± 0.6038	35.53 ± 3.29	<0.0001
Number of living children	0.6000 ± 0.4900	0.4667 ± 0.6182	0.3665

Table 6 Details of the individual with early-onset preeclampsia or late-onset preeclampsia included in the study

Parameters	Early-onset preeclampsia (n=11)	Late-onset preeclampsia (n=19)	p Value
The gestational week when blood pressure begins to rise	28.82± 2.8220	36.05± 1.129	< 0.0001
Age (years)	32.45± 4.6768	32.36± 3.8472	0.9568
BMI (kg/m^2)	29.64± 2.6840	28.71±4.4506	0.5388
Gestational age (weeks)	33.45± 3.7887	36.77± 1.2171	0.0014
Number of living children	0.36± 0.5045	0.36 ± 0.4956	0.98

Figure 1

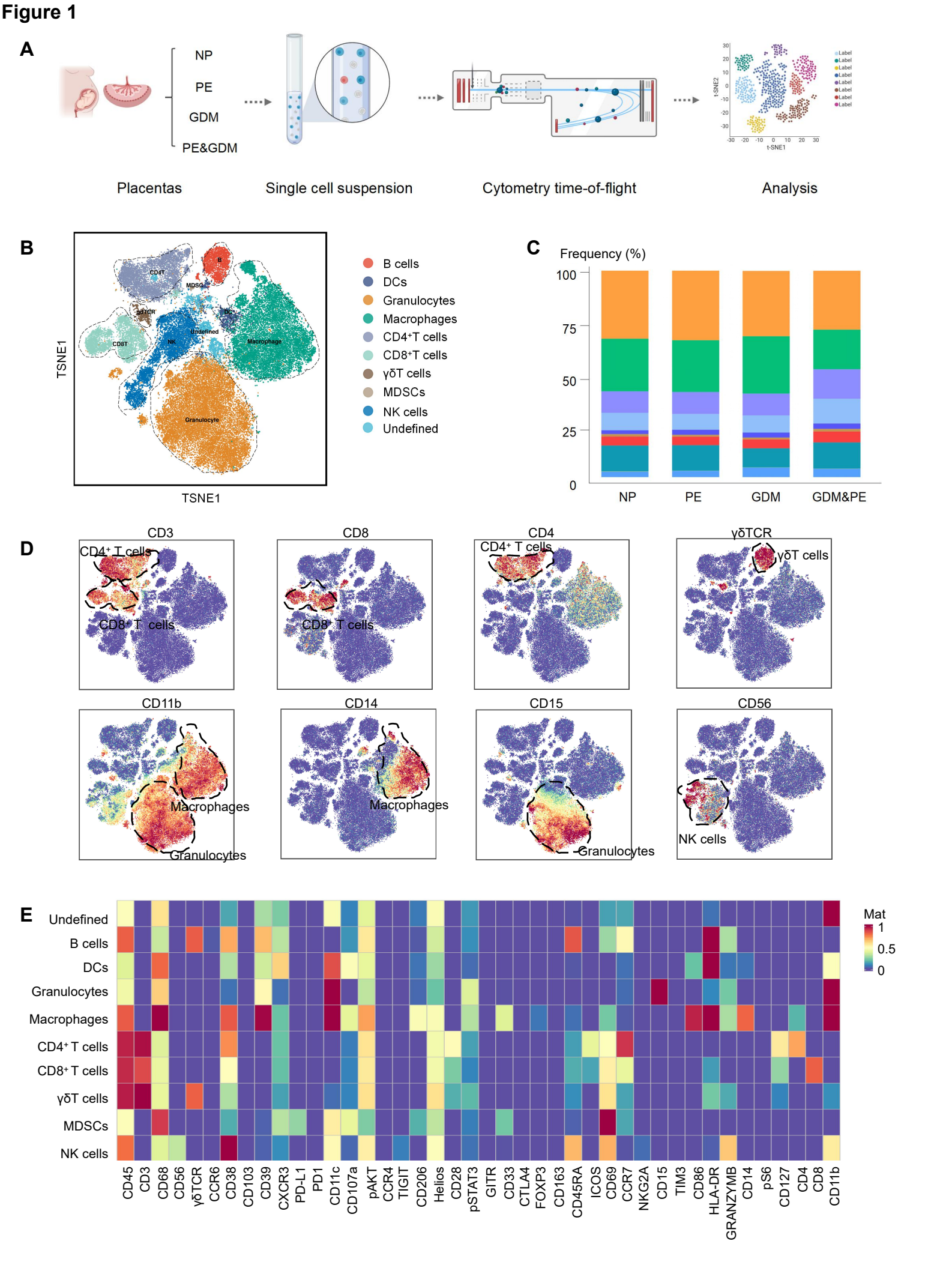
A
NP
PE
GDM
PE&GDM
Placentas
Single cell suspension
Cytometry time-of-flight
Analysis
B
TSNE1
TSNE1
B cells
DCs
Granulocytes
Macrophages
CD4⁺T cells
CD8⁺T cells
γδT cells
MDSCs
NK cells
Undefined
C
Frequency (%)
100
75
50
25
0
NP
PE
GDM
GDM&PE
D
CD3
CD4⁺ T cells
CD8⁺ T cells
CD8
CD8⁺ T cells
CD4
CD4⁺ T cells
γδTCR
γδT cells
CD11b
Macrophages
Granulocytes
CD14
Macrophages
CD15
Granulocytes
CD56
NK cells
E
Undefined
B cells
DCs
Granulocytes
Macrophages
CD4⁺ T cells
CD8⁺ T cells
γδT cells
MDSCs
NK cells
CD45
CD3
CD68
CD56
γδTCR
CCR6
CD38
CD103
CD39
CXCR3
PD-L1
PD1
CD11c
CD107a
pAKT
CCR4
TIGIT
CD206
Helios
CD28
pSTAT3
GITR
CD33
CTLA4
FOXP3
CD163
CD45RA
ICOS
CD69
CCR7
NKG2A
CD15
TIM3
CD86
HLA-DR
GRANZYMB
CD14
pS6
CD127
CD4
CD8
CD11b
Mat
1
0.5
0

Figure 2

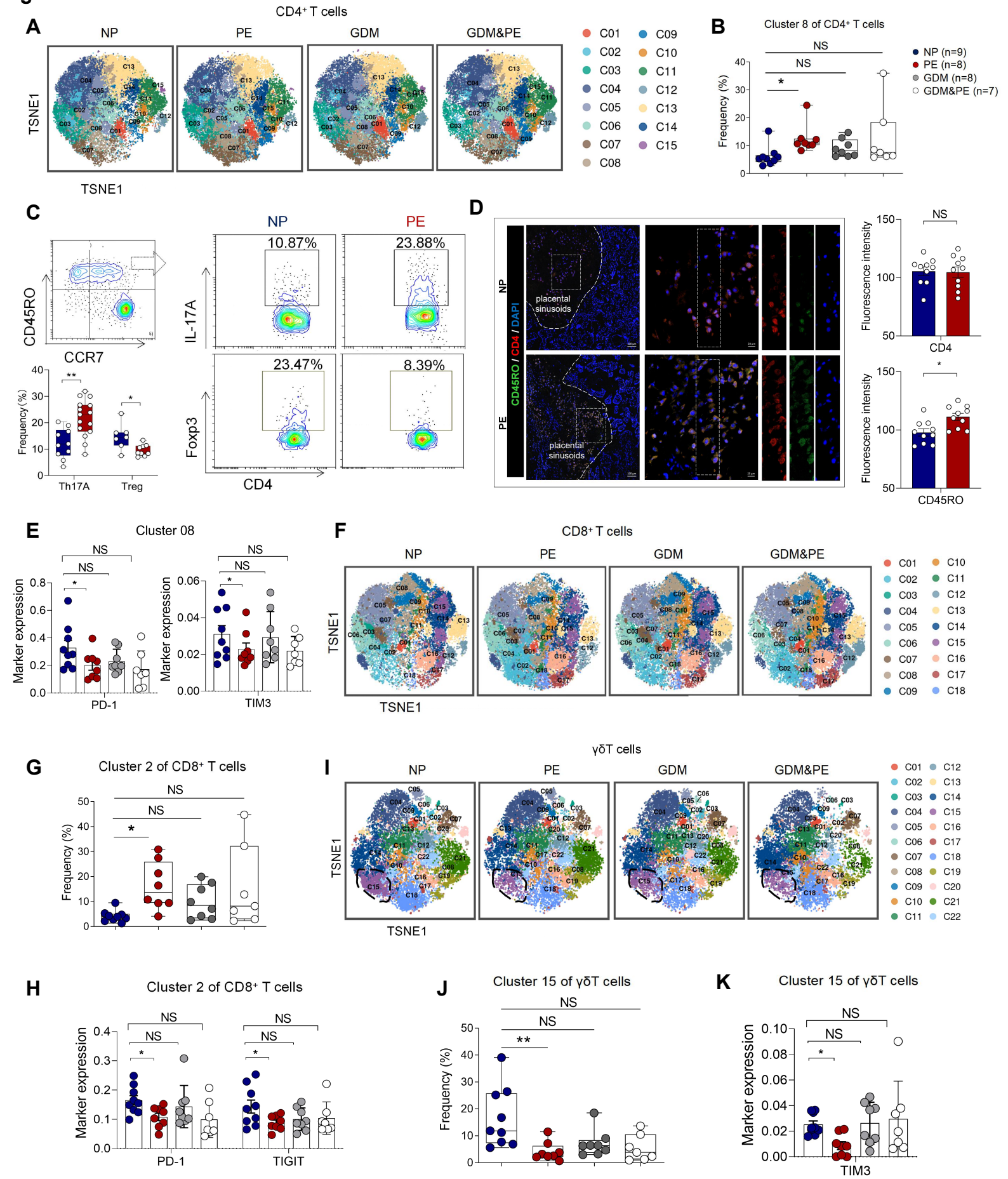
A
CD4+ T cells
NP
PE
GDM
GDM&PE
TSNE1
TSNE1
C01 C02 C03 C04 C05 C06 C07 C08 C09 C10 C11 C12 C13 C14 C15
B
Cluster 8 of CD4+ T cells
NP (n=9)
PE (n=8)
GDM (n=8)
GDM&PE (n=7)
Frequency (%)
NS
NS
*
C
CD45RO
CCR7
Frequency (%)
Th17A
Treg
NP
PE
10.87%
23.88%
23.47%
8.39%
IL-17A
Foxp3
CD4
D
NP
PE
CD45RO / CD4 / DAPI
placental sinusoids
placental sinusoids
Fluorescence intensity
CD4
CD45RO
E
Cluster 08
Marker expression
PD-1
TIM3
F
CD8+ T cells
NP
PE
GDM
GDM&PE
TSNE1
TSNE1
C01 C02 C03 C04 C05 C06 C07 C08 C09 C10 C11 C12 C13 C14 C15 C16 C17 C18
G
Cluster 2 of CD8+ T cells
Frequency (%)
I
γδT cells
NP
PE
GDM
GDM&PE
TSNE1
TSNE1
C01 C02 C03 C04 C05 C06 C07 C08 C09 C10 C11 C12 C13 C14 C15 C16 C17 C18 C19 C20 C21 C22
H
Cluster 2 of CD8+ T cells
Marker expression
PD-1
TIGIT
J
Cluster 15 of γδT cells
Frequency (%)
K
Cluster 15 of γδT cells
Marker expression
TIM3

Figure 2 figure supplement 1

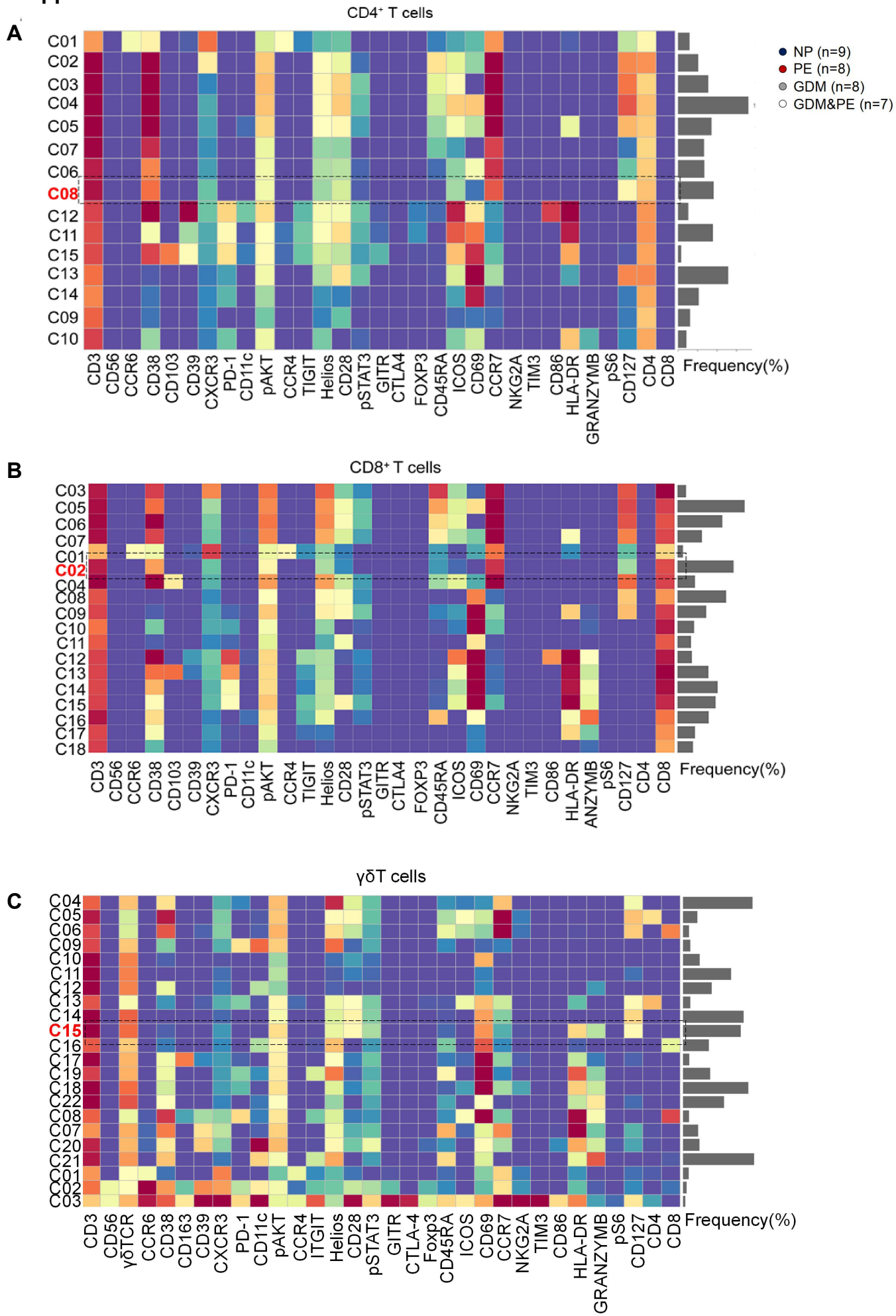

Figure 3

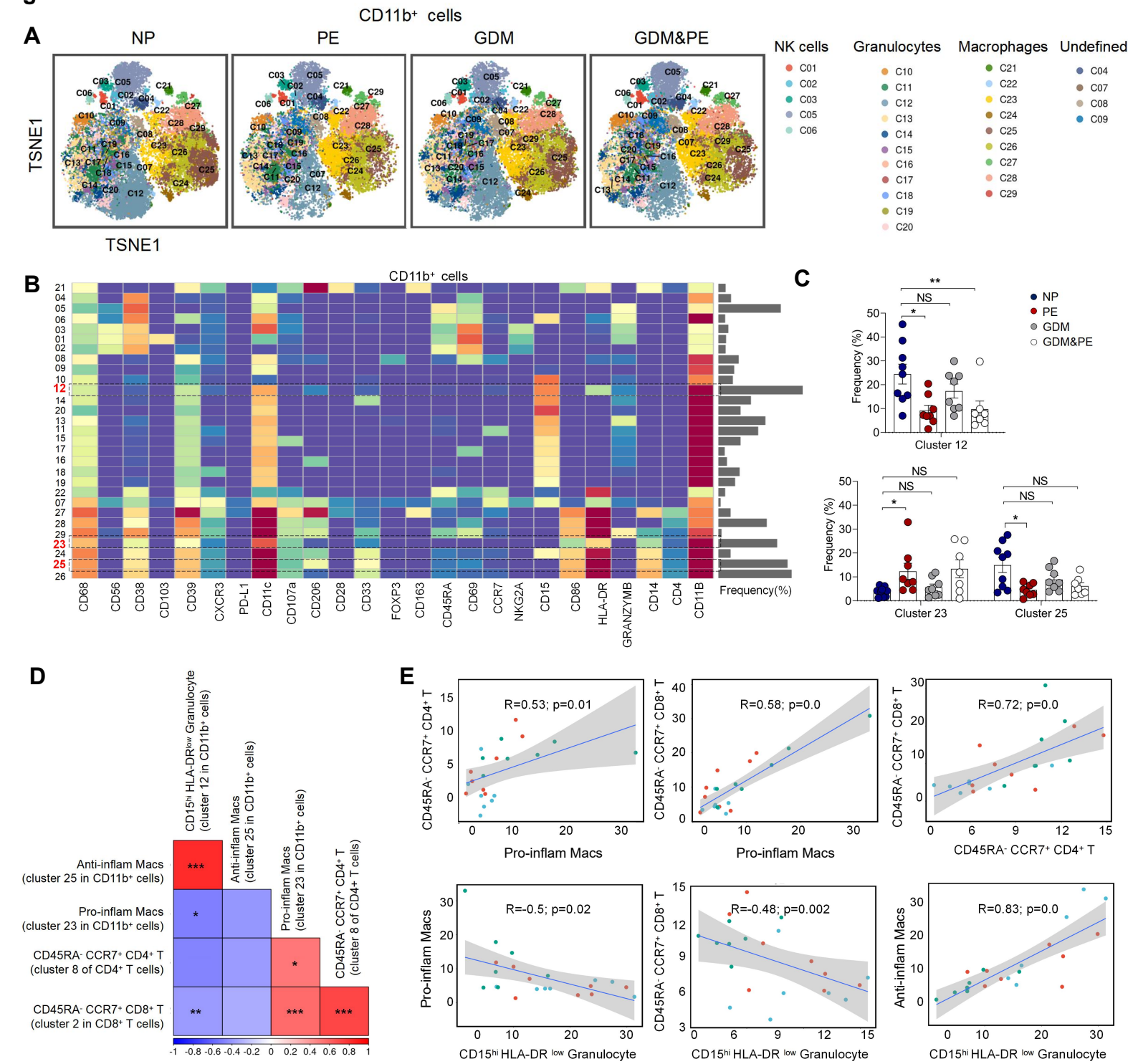
A
CD11b+ cells
NP
PE
GDM
GDM&PE
TSNE1
TSNE1
NK cells
C01
C02
C03
C05
C06
Granulocytes
C10
C11
C12
C13
C14
C15
C16
C17
C18
C19
C20
Macrophages
C21
C22
C23
C24
C25
C26
C27
C28
C29
Undefined
C04
C07
C08
C09
B
CD11b+ cells
CD68
CD56
CD38
CD103
CD39
CXCR3
PD-L1
CD11c
CD107a
CD206
CD28
CD33
FOXP3
CD163
CD45RA
CD69
CCR7
NKG2A
CD15
CD86
HLA-DR
GRANZYMB
CD14
CD4
CD11B
Frequency(%)
C
NP
PE
GDM
GDM&PE
Frequency (%)
Cluster 12
Cluster 23
Cluster 25
NS
D
CD15hi HLA-DRlow Granulocyte (cluster 12 in CD11b+ cells)
Anti-inflam Macs (cluster 25 in CD11b+ cells)
Pro-inflam Macs (cluster 23 in CD11b+ cells)
CD45RA- CCR7+ CD4+ T (cluster 8 of CD4+ T cells)
Anti-inflam Macs (cluster 25 in CD11b+ cells)
Pro-inflam Macs (cluster 23 in CD11b+ cells)
CD45RA- CCR7+ CD4+ T (cluster 8 of CD4+ T cells)
CD45RA- CCR7+ CD8+ T (cluster 2 in CD8+ T cells)
E
R=0.53; p=0.01
R=0.58; p=0.0
R=0.72; p=0.0
R=-0.5; p=0.02
R=-0.48; p=0.002
R=0.83; p=0.0
Pro-inflam Macs
CD45RA- CCR7+ CD4+ T
CD45RA- CCR7+ CD8+ T
Anti-inflam Macs
CD15hi HLA-DR low Granulocyte

Figure 4

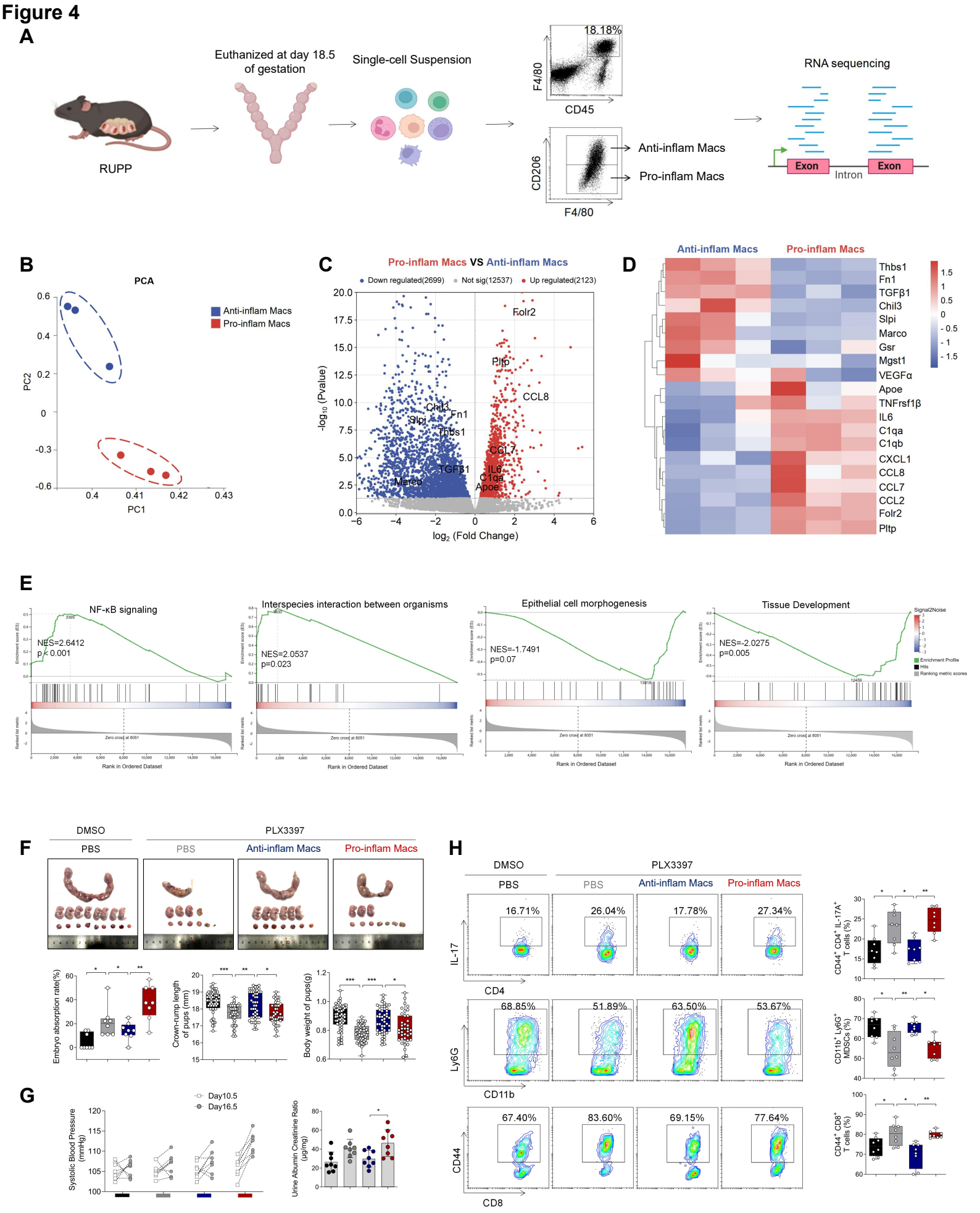
A
RUPP
Euthanized at day 18.5 of gestation
Single-cell Suspension
18.18%
F4/80
CD45
CD206
F4/80
Anti-inflam Macs
Pro-inflam Macs
RNA sequencing
Exon
Intron
Exon
B
PCA
Anti-inflam Macs
Pro-inflam Macs
PC2
PC1
C
Pro-inflam Macs VS Anti-inflam Macs
Down regulated(2699)
Not sig(12537)
Up regulated(2123)
-log10 (Pvalue)
log2 (Fold Change)
Folr2
Pltp
CCL8
Chil3
Fn1
Slpi
Thbs1
CCL7
TGFβ1
IL6
C1qa
Marco
Apoe
D
Anti-inflam Macs
Pro-inflam Macs
Thbs1
Fn1
TGFβ1
Chil3
Slpi
Marco
Gsr
Mgst1
VEGFα
Apoe
TNFrsf1β
IL6
C1qa
C1qb
CXCL1
CCL8
CCL7
CCL2
Folr2
Pltp
E
NF-κB signaling
NES=2.6412
p< 0.001
Interspecies interaction between organisms
NES=2.0537
p=0.023
Epithelial cell morphogenesis
NES=-1.7491
p=0.07
Tissue Development
NES=-2.0275
p=0.005
Rank in Ordered Dataset
F
DMSO
PLX3397
PBS
PBS
Anti-inflam Macs
Pro-inflam Macs
Embryo absorption rate(%)
Crown-rump length of pups (mm)
Body weight of pups(g)
G
Day10.5
Day16.5
Systolic Blood Pressure (mmHg)
Urine Albumin Creatinine Ratio (μg/mg)
H
DMSO
PLX3397
PBS
PBS
Anti-inflam Macs
Pro-inflam Macs
16.71%
26.04%
17.78%
27.34%
IL-17
CD4
68.85%
51.89%
63.50%
53.67%
Ly6G
CD11b
67.40%
83.60%
69.15%
77.64%
CD44
CD8
CD44+ CD4+ IL-17A+ T cells (%)
CD11b+ Ly6G+ MDSCs (%)
CD44+ CD8+ T cells (%)

Figure 4 figure supplement 1

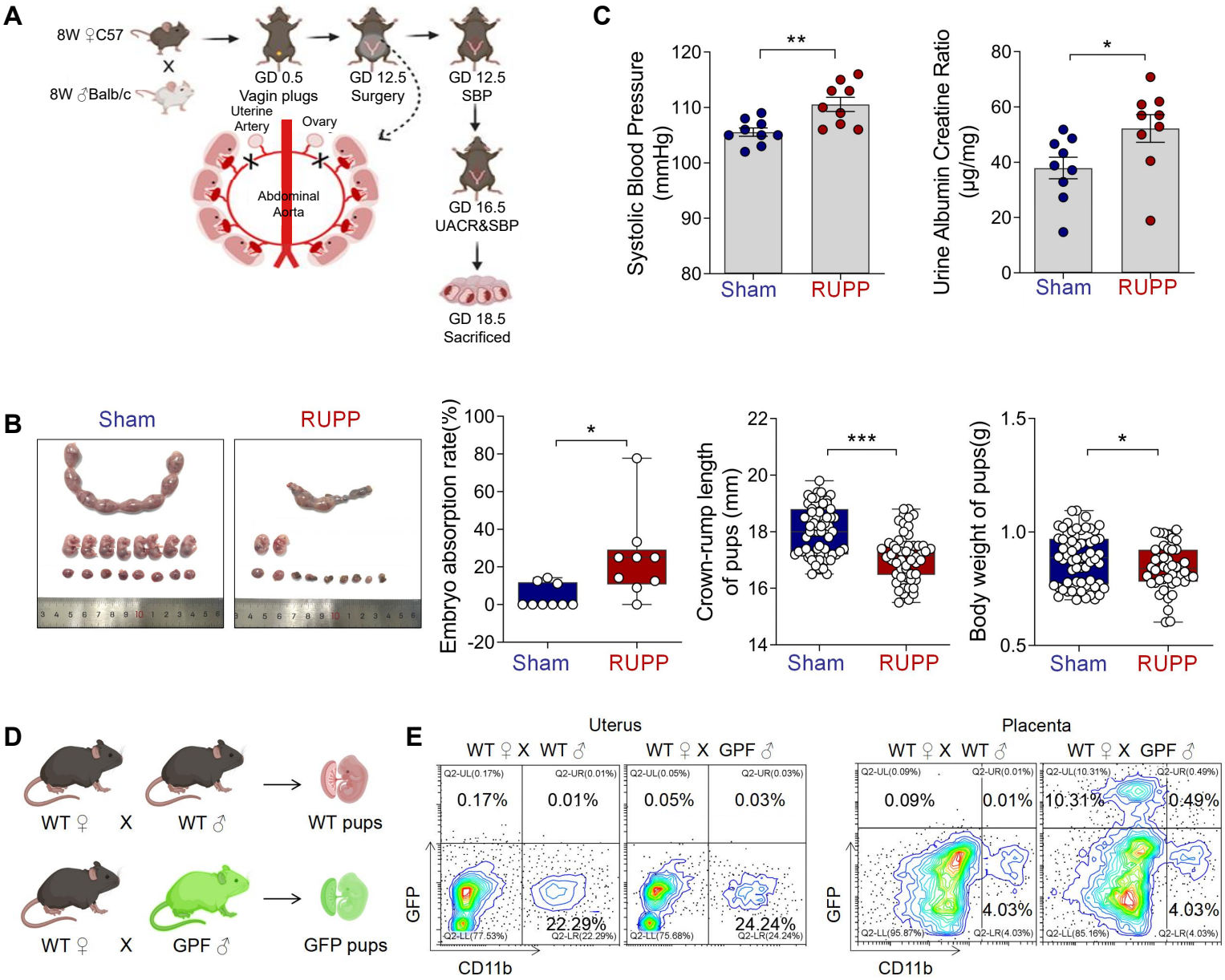

Figure 4 figure supplement 2

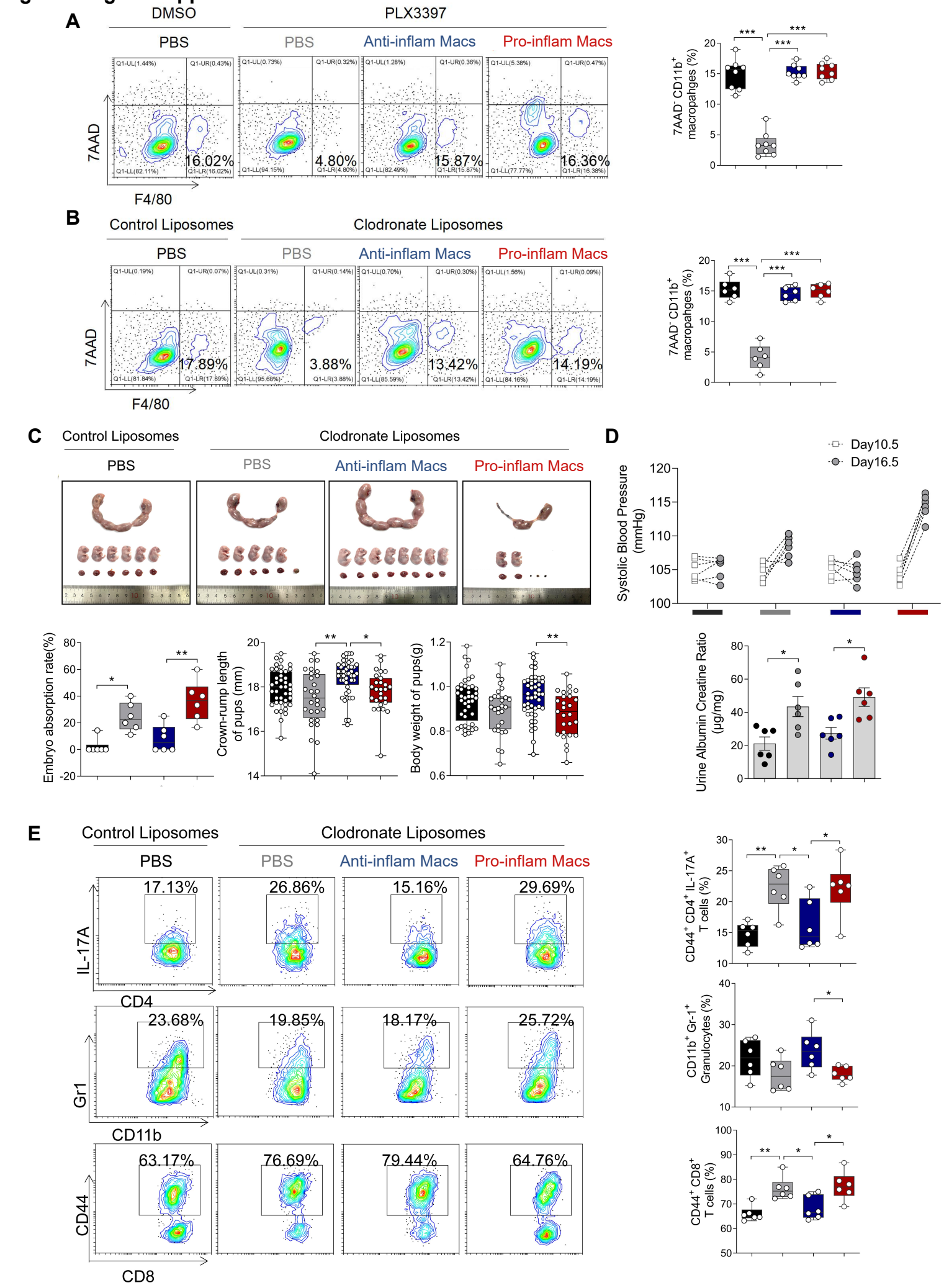

Figure 5

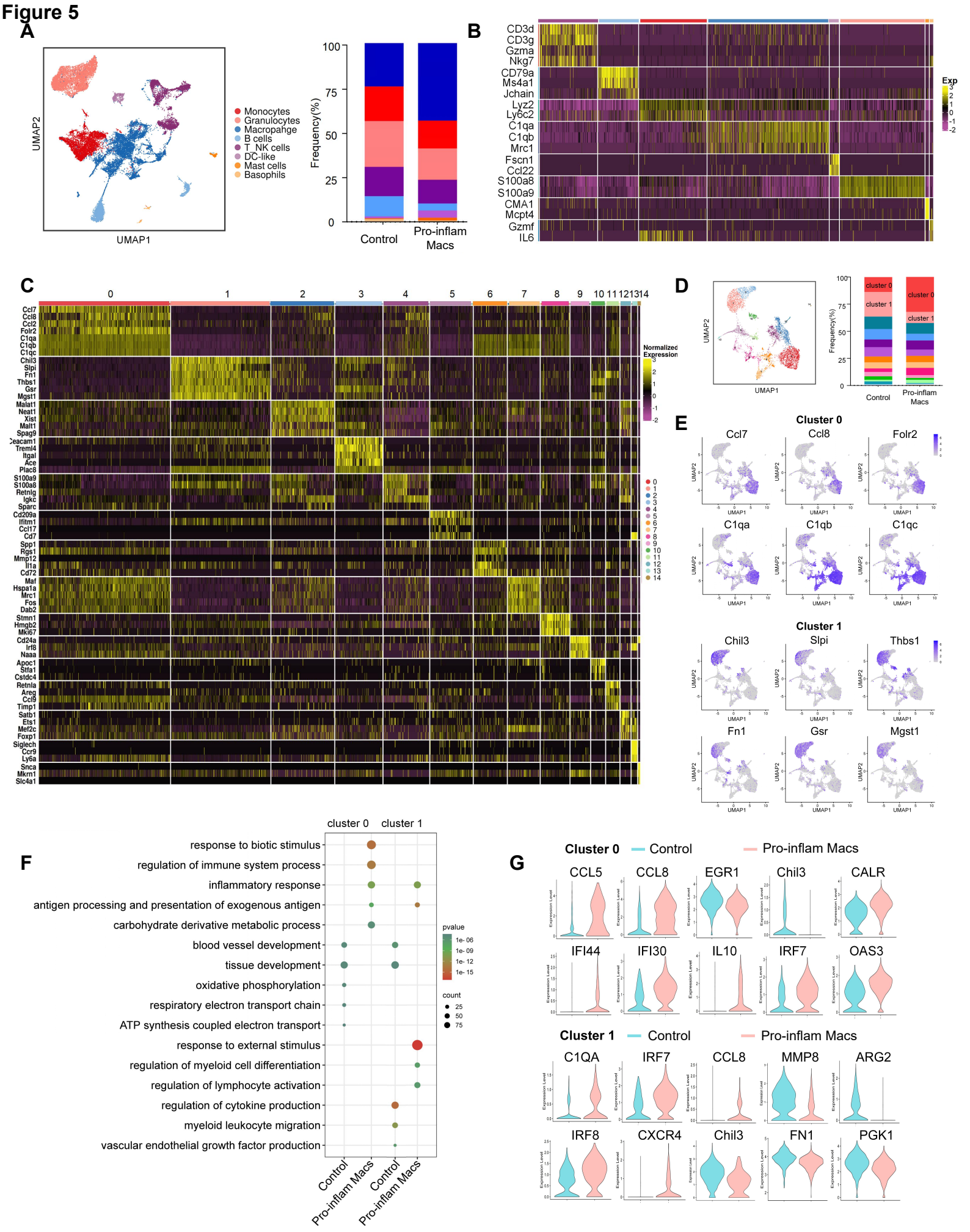
A
UMAP2
UMAP1
Monocytes
Granulocytes
Macropahge
B cells
T_NK cells
DC-like
Mast cells
Basophils
Frequency(%)
Control
Pro-inflam Macs
B
CD3d
CD3g
Gzma
Nkg7
CD79a
Ms4a1
Jchain
Lyz2
Ly6c2
C1qa
C1qb
Mrc1
Fscn1
Ccl22
S100a8
S100a9
CMA1
Mcpt4
Gzmf
IL6
Exp
C
Normalized Expression
D
cluster 0
cluster 1
E
Cluster 0
Ccl7
Ccl8
Folr2
C1qa
C1qb
C1qc
Cluster 1
Chil3
Slpi
Thbs1
Fn1
Gsr
Mgst1
F
cluster 0
cluster 1
response to biotic stimulus
regulation of immune system process
inflammatory response
antigen processing and presentation of exogenous antigen
carbohydrate derivative metabolic process
blood vessel development
tissue development
oxidative phosphorylation
respiratory electron transport chain
ATP synthesis coupled electron transport
response to external stimulus
regulation of myeloid cell differentiation
regulation of lymphocyte activation
regulation of cytokine production
myeloid leukocyte migration
vascular endothelial growth factor production
pvalue
count
Control
Pro-inflam Macs
G
Cluster 0
Control
Pro-inflam Macs
CCL5
CCL8
EGR1
Chil3
CALR
IFI44
IFI30
IL10
IRF7
OAS3
Cluster 1
C1QA
IRF7
CCL8
MMP8
ARG2
IRF8
CXCR4
Chil3
FN1
PGK1

Figure 6

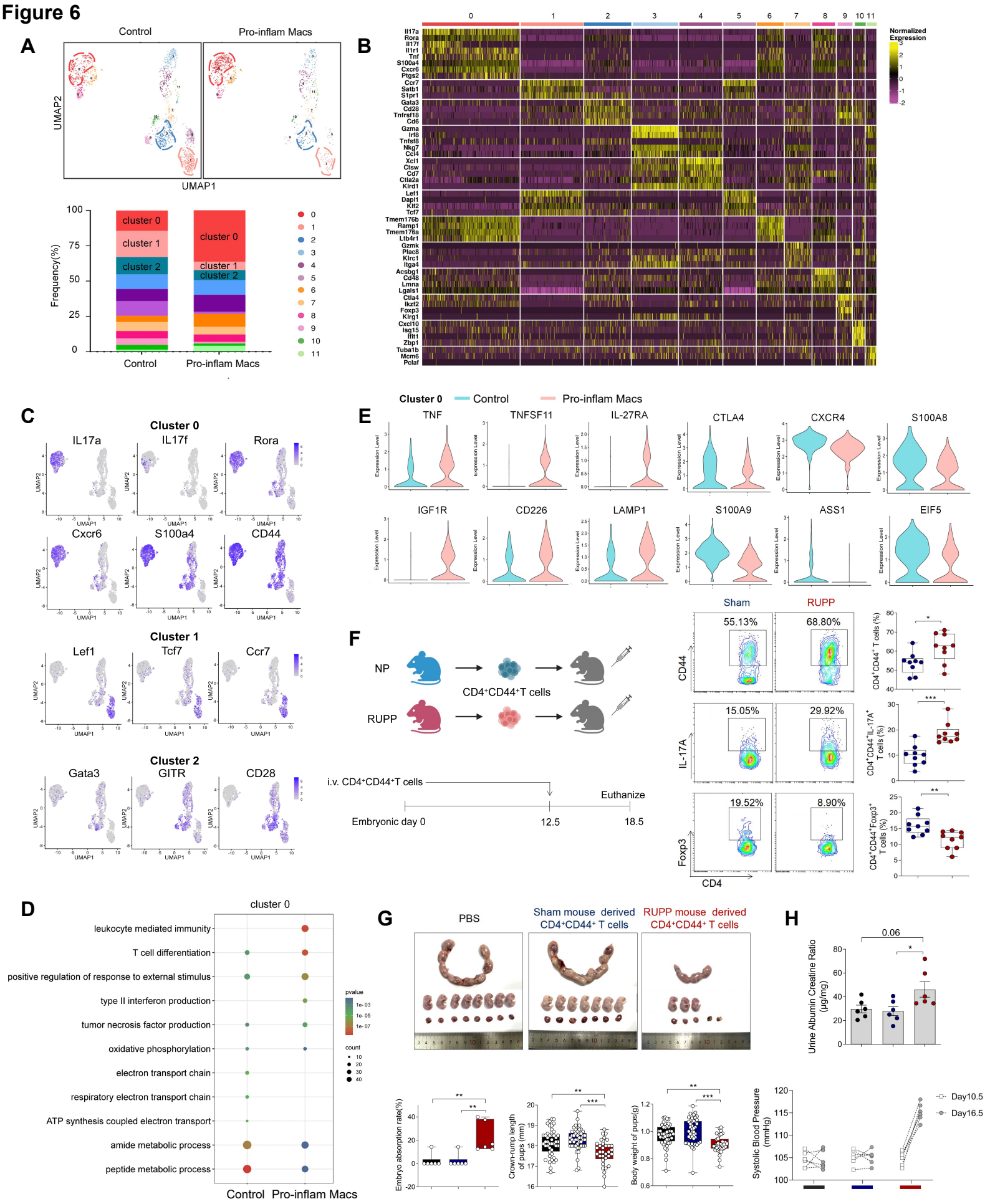
A
Control
Pro-inflam Macs
UMAP2
UMAP1
Frequency(%)
cluster 0
cluster 1
cluster 2
B
Normalized Expression
C
Cluster 0
IL17a
IL17f
Rora
Cxcr6
S100a4
CD44
Cluster 1
Lef1
Tcf7
Ccr7
Cluster 2
Gata3
GITR
CD28
D
cluster 0
leukocyte mediated immunity
T cell differentiation
positive regulation of response to external stimulus
type II interferon production
tumor necrosis factor production
oxidative phosphorylation
electron transport chain
respiratory electron transport chain
ATP synthesis coupled electron transport
amide metabolic process
peptide metabolic process
pvalue
count
Control
Pro-inflam Macs
E
Cluster 0
Control
Pro-inflam Macs
TNF
TNFSF11
IL-27RA
CTLA4
CXCR4
S100A8
IGF1R
CD226
LAMP1
S100A9
ASS1
EIF5
Expression Level
F
NP
RUPP
CD4⁺CD44⁺T cells
i.v. CD4⁺CD44⁺T cells
Euthanize
Embryonic day 0
12.5
18.5
Sham
RUPP
55.13%
68.80%
15.05%
29.92%
19.52%
8.90%
CD44
IL-17A
Foxp3
CD4
CD4⁺CD44⁺ T cells (%)
CD4⁺CD44⁺IL-17A⁺ T cells (%)
CD4⁺CD44⁺Foxp3⁺ T cells (%)
G
PBS
Sham mouse derived CD4⁺CD44⁺ T cells
RUPP mouse derived CD4⁺CD44⁺ T cells
Embryo absorption rate(%)
Crown-rump length of pups (mm)
Body weight of pups(g)
H
Urine Albumin Creatine Ratio (μg/mg)
0.06
Systolic Blood Pressure (mmHg)
Day10.5
Day16.5

Figure 6 figure supplement 1

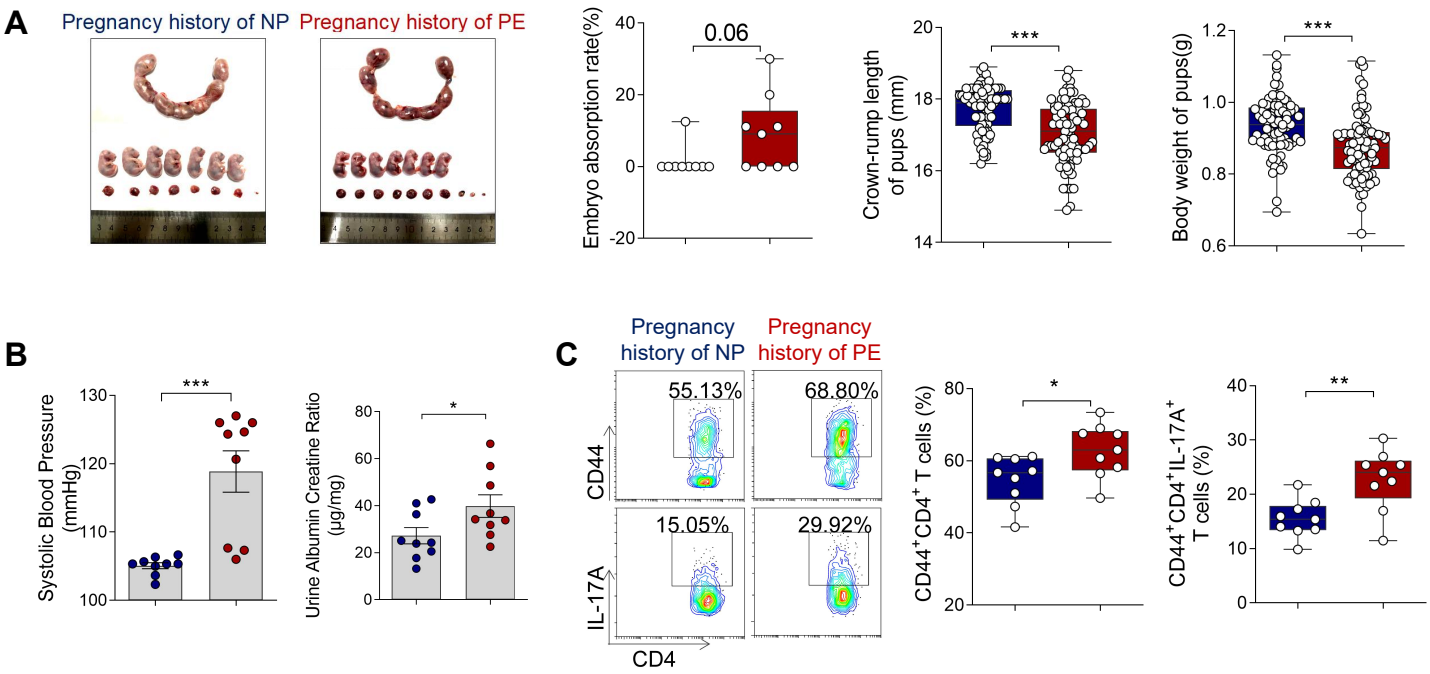

Figure 6 figure supplement 2

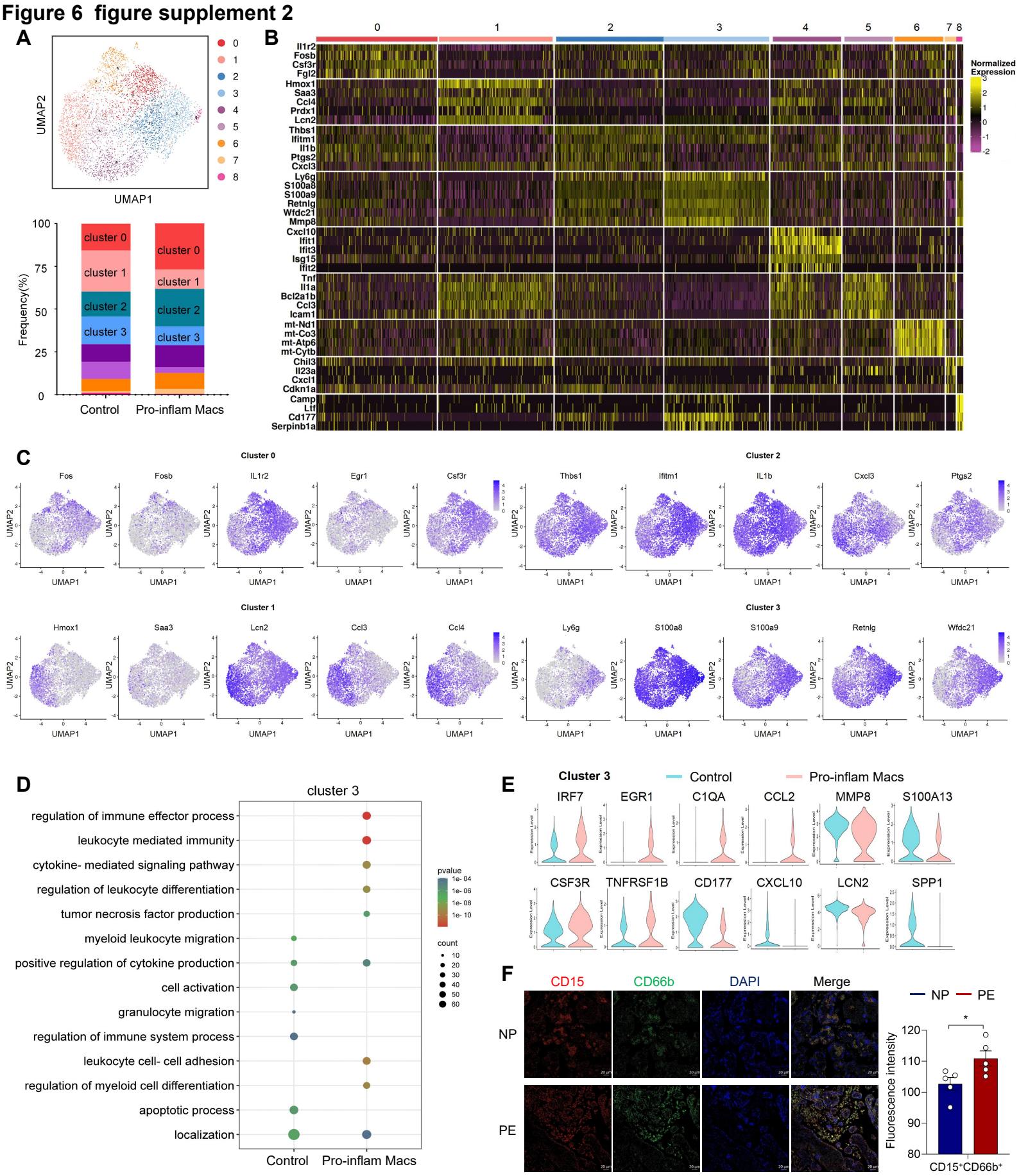

Figure 7

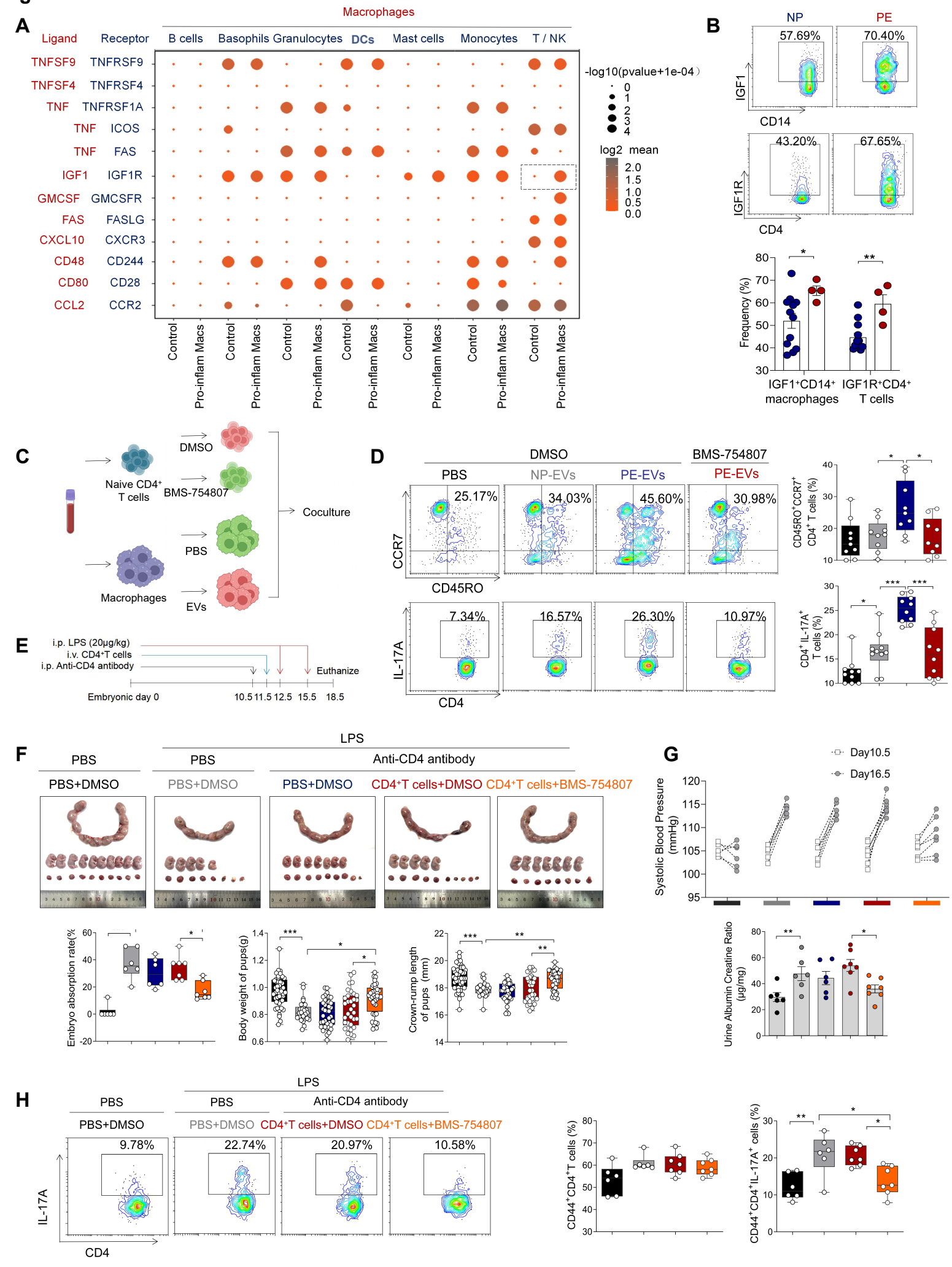
A
Macrophages
Ligand
Receptor
B cells
Basophils
Granulocytes
DCs
Mast cells
Monocytes
T / NK
TNFSF9 TNFRSF9
TNFSF4 TNFRSF4
TNF TNFRSF1A
TNF ICOS
TNF FAS
IGF1 IGF1R
GMCSF GMCSFR
FAS FASLG
CXCL10 CXCR3
CD48 CD244
CD80 CD28
CCL2 CCR2
Control
Pro-inflam Macs
-log10(pvalue+1e-04)
log2 mean
B
NP
PE
57.69%
70.40%
IGF1
CD14
43.20%
67.65%
IGF1R
CD4
Frequency (%)
IGF1+CD14+ macrophages
IGF1R+CD4+ T cells
C
DMSO
Naive CD4+ T cells
BMS-754807
Coculture
PBS
Macrophages
EVs
D
DMSO
BMS-754807
PBS
NP-EVs
PE-EVs
PE-EVs
25.17%
34.03%
45.60%
30.98%
CCR7
CD45RO
CD45RO+CCR7+ CD4+ T cells (%)
7.34%
16.57%
26.30%
10.97%
IL-17A
CD4
CD4+ IL-17A+ T cells (%)
E
i.p. LPS (20μg/kg)
i.v. CD4+T cells
i.p. Anti-CD4 antibody
Euthanize
Embryonic day 0
10.5 11.5 12.5 15.5 18.5
F
LPS
PBS
PBS
Anti-CD4 antibody
PBS+DMSO
PBS+DMSO
PBS+DMSO
CD4+T cells+DMSO
CD4+T cells+BMS-754807
Embryo absorption rate(%
Body weight of pups(g)
Crown-rump length of pups (mm)
G
Day10.5
Day16.5
Systolic Blood Pressure (mmHg)
Urine Albumin Creatine Ratio (μg/mg)
H
LPS
PBS
PBS
Anti-CD4 antibody
PBS+DMSO
PBS+DMSO
CD4+T cells+DMSO
CD4+T cells+BMS-754807
9.78%
22.74%
20.97%
10.58%
IL-17A
CD4
CD44+CD4+T cells (%)
CD44+CD4+IL-17A+ cells (%)
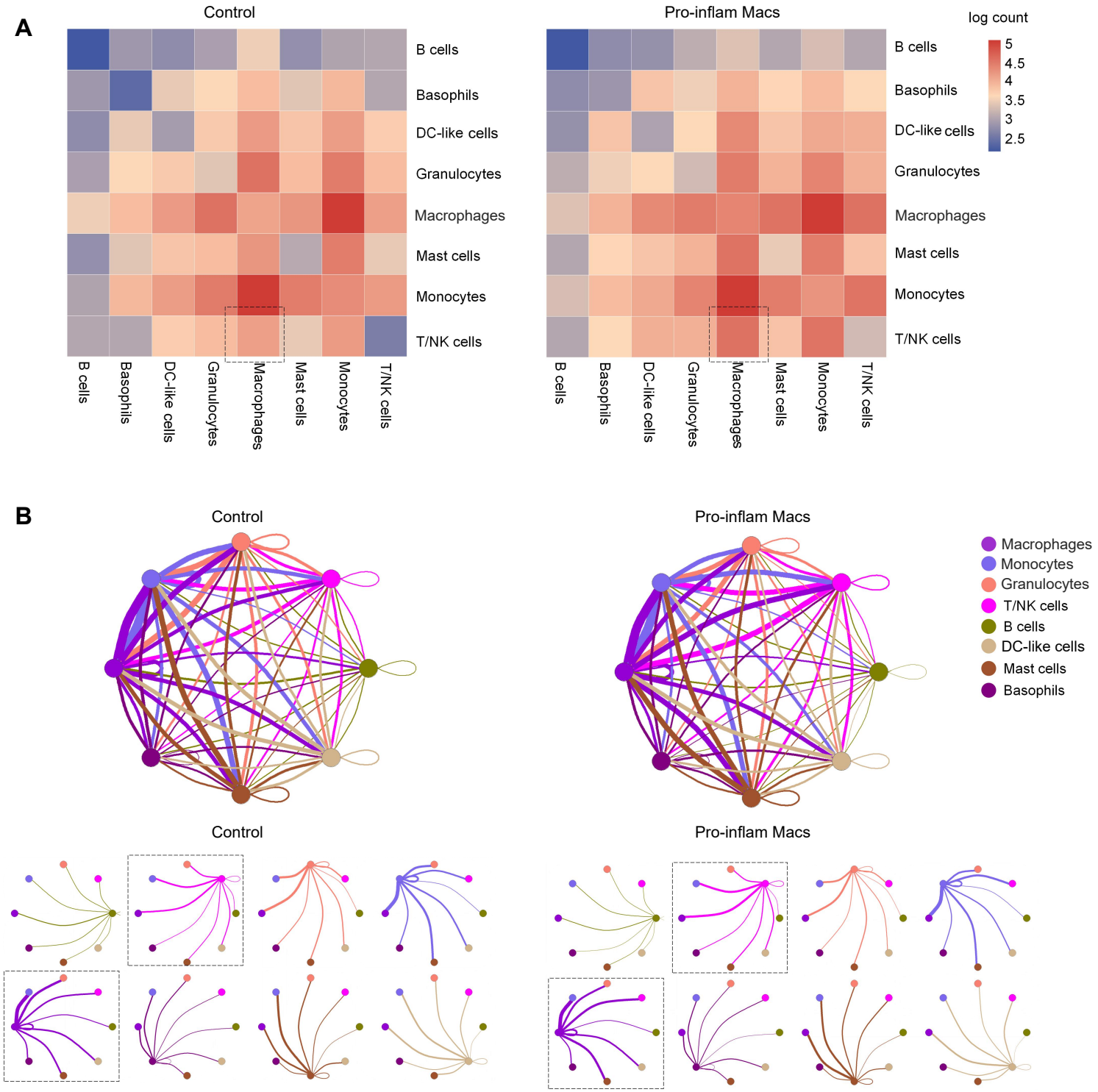
Figure 7 figure supplement 1